

AD-A232 965

MARTIN MARIETTA

MML TR 91-10c

(12)

**A STUDY OF THE INFLUENCE OF ALLOYING
ADDITIONS ON THE PASSIVITY OF ALUMINUM**

Annual Report

December 1, 1989 - November 30, 1990

Submitted to:

**Office of Naval Research
800 North Quincy Street
Arlington, VA 22217-5000**

**DTIC
ELECTE
MAR 08 1991
S E D**

Submitted by:

**G.D. Davis, T.L. Fritz, and B.J. Rees
Martin Marietta Laboratories, Baltimore, MD 21227**

**B.A. Shaw
The Pennsylvania State University, State College, PA 16802**

**and W.C. Moshier
Martin Marietta Space Systems, Denver, CO 80201**

March 1, 1991

DISTRIBUTION STATEMENT A
Approved for public release; Distribution Unlimited

91 3 07 086



MML TR 91-10c

Accession For	
NTIS GRA&I	<input checked="" type="checkbox"/>
DTIC TAB	<input type="checkbox"/>
Unannounced	<input type="checkbox"/>
Justification	
By _____	
Distribution/	
Availability Codes	
Dist	Avail and/or Special
A-1	

**A STUDY OF THE INFLUENCE OF ALLOYING
ADDITIONS ON THE PASSIVITY OF ALUMINUM**

Annual Report

December 1, 1989 - November 30, 1990

Submitted to:

**Office of Naval Research
800 North Quincy Street
Arlington, VA 22217-5000**

Submitted by:

**G.D. Davis, T.L. Fritz, and B.J. Rees
Martin Marietta Laboratories, Baltimore, MD 21227**

**B.A. Shaw
The Pennsylvania State University, State College, PA 16802**

**and W.C. Moshier
Martin Marietta Space Systems, Denver, CO 80201**

March 1, 1991

DISTRIBUTION STATEMENT A
Approved for public release; Distribution Unlimited

REPORT DOCUMENTATION PAGE

1a REPORT SECURITY CLASSIFICATION Unclassified			1b RESTRICTIVE MARKINGS None	
2a SECURITY CLASSIFICATION AUTHORITY			3 DISTRIBUTION AVAILABILITY OF REPORT Unlimited	
2b DECLASSIFICATION/DOWNGRADING SCHEDULE None				
4 PERFORMING ORGANIZATION REPORT NUMBER(S) MML TR 91-10c			5 MONITORING ORGANIZATION REPORT NUMBER(S)	
6a NAME OF PERFORMING ORGANIZATION Martin Marietta Corporation Martin Marietta Laboratories		6b OFFICE SYMBOL (If applicable) MML		7a NAME OF MONITORING ORGANIZATION Defense Contract Administration Services Management Area - Baltimore
6c ADDRESS (City, State, and ZIP Code) 1450 South Rolling Road Baltimore, Maryland 21227-3898			7b ADDRESS (City, State, and ZIP Code) 300 East Joppa Road Baltimore, Maryland 21204-3099	
8a NAME OF FUNDING SPONSORING ORGANIZATION Office of Naval Research		8b OFFICE SYMBOL (If applicable) ONR		9 PROCUREMENT INSTRUMENT IDENTIFICATION NUMBER N00014-85-C-0638
8c ADDRESS (City, State, and ZIP Code) 800 North Quincy Street Arlington, VA 22217-5000			10 SOURCE OF FUNDING NUMBERS	
			PROGRAM ELEMENT NO	PROJECT NO
			TASK NO	WORK UNIT ACCESSION NO
11 TITLE (Include Security Classification) A Study of the Influence of Alloying Additions on the Passivity of Aluminum				
12 PERSONAL AUTHOR(S) G.D. Davis, T.L. Fritz, B.J. Rees, B.A. Shaw and W.C. Moshier				
13a TYPE OF REPORT Annual	13b TIME COVERED FROM 12/1/89 TO 11/30/90	14 DATE OF REPORT (Year, Month, Day) March 1, 1991		15 PAGE COUNT
16 SUPPLEMENTARY NOTATION				
17 COSATI CODES			18 SUBJECT TERMS (Continue on reverse if necessary and identify by block number)	
FIELD	GROUP	SUB-GROUP	Approved for public release; distribution unlimited. Reproduction in whole or in part is permitted for any purpose of the United States Government.	
19 ABSTRACT (Continue on reverse if necessary and identify by block number) Whereas supersaturated aluminum alloys demonstrate enhanced passivity, conventional aluminum alloys spontaneously pit in air-saturated chloride solutions. Under ONR program N00014-85-C-0638, we have investigated the mechanisms involved in several of these alloys. In the 1990 contract year, we have concentrated on three areas: evaluation and characterization of Al-W alloys, which exhibit the best corrosion performance of any alloy system studied to date; characterization of the passive-film structure of Al-Mo alloys; and production and characterization of Al-W and Al-Ta powders, which will be used for compaction into bulk material. Surface analysis of the Al-W passive films formed during polarization show surprising little oxidized solute compared to other alloys. These results indicate that the barrier-layer formation and electrostatic repulsion mechanisms used to explain the passivity of other alloys are not involved here. Instead the W may act to stabilize the passive film structure in a way similar to the way Mo acts in Al-Mo alloys. That is, the oxidized molybdenum reduces the concentration of unstable tetrahedrally coordinated atomic sites, as suggested by reflection				
20 DISTRIBUTION AVAILABILITY OF ABSTRACT <input type="checkbox"/> UNCLASSIFIED UNLIMITED <input type="checkbox"/> SAME AS RPT <input type="checkbox"/> DTIC USERS			21 ABSTRACT SECURITY CLASSIFICATION Unclassified	
22 NAME OF RESPONSIBLE INDIVIDUAL Dr. Guy D. Davis			23 REPORT NUMBER (Include Access Code) 301-247-0700 X 2378	

19. Abstract

extended x-ray absorption fine structure (reflEXAFS) measurements. Finally, characterization of Al-Ta and Al-W powders indicate that some solute precipitates, but most remains in solid solution. Although such precipitation degrades passivity in cosputter-deposited alloys, the alloys still exhibit superior passivity compared to conventional materials. Characterization of the corrosion behavior of bulk material formed from these powders is ongoing.

Contents

1 INTRODUCTION	2
2 EXPERIMENTAL PROCEDURE	5
2.1 Al-W (Co)sputter-Deposited Alloys	5
2.2 Al-Mo Cosputter-Deposited Alloys	9
3 RESULTS AND DISCUSSION	11
3.1 Sputter-Deposited Al-W Alloys	11
3.2 reflEXAFS Measurements	28
3.3 Powder Production and Characterization	37
4 SUMMARY AND CONCLUSIONS	43
5 REFERENCES	46
6 PUBLICATIONS DURING THE 1990 CONTRACT YEAR	50
7 PRESENTATIONS DURING THE 1990 CONTRACT YEAR	51
8 OTHER RELATED ACTIVITIES DURING THE 1990 CONTRACT YEAR	52

List of Figures

1.1	Polarization curves for elemental Al and several supersaturated Al alloys in aerated 0.1 N KCl.	3
3.1	Glancing angle x-ray diffraction patterns for sputter-deposited Al cosputter-deposited Al-7%W and sputter-deposited Al-1.5%W alloys.	12
3.2	Glancing angle x-ray diffraction patterns for a sputter-deposited Al-5%W alloy heat treated at 400°C for 1 hour and sputter-deposited Al-1.5%W alloys heat treated at 400°C for either 1 or 24 hours.	13
3.3	Selected area electron diffraction patterns for Al-W specimens taken from the right-hand side and the center of a cosputter-deposited wafer.	15
3.4	Pitting potentials as a function of Al-W alloy concentration.	16
3.5	Anodic polarization behavior of Al-W alloys in aerated 0.1M KCl compared to Al-8%Mo, pure aluminum, and pure W.	18
3.6	Anodic polarization behavior in aerated 0.1M KCl for duplicate Al-5%W specimens heat treated for 1 hour at 400°C compared to a polarization curve for a non-heat treated Al-5%W specimen.	19
3.7	Anodic polarization behavior in aerated 0.1 M KCl for Al-1.5%W alloys heat treated at 400°C for either 1 or 24 hours.	20

3.8	Surface composition as measured by XPS for an Al-6W alloy as a function of applied potential	22
3.9	Surface composition as measured by XPS for an Al-1.5W alloy as a function of applied potential	23
3.10	Al 2p and W 4f spectra for the Al-6W alloy at different applied potentials.	24
3.11	Potentiodynamic scans of a) Al-6%Mo and pure Al in 0.1 M KCl and b) TAA Al and unanodized pure Al in 0.05 M Na ₂ SO ₄ with 1000 ppm Cl ⁻	29
3.12	Reflectivity spectra measured from single-crystal corundum at seven different reflection angles.	31
3.13	Magnitude of the Fourier transform of the reflEXAFS data for corundum, uncorrected for phase.	32
3.14	Magnitude of the Fourier transform of the data for the passive film on Al-11%Mo, uncorrected for phase.	33
3.15	SEM micrographs of atomized Al, Al-0.56%W, and Al-0.32%Ta powders.	39
3.16	XRD results for atomized Al-0.56%W and Al-0.32%Ta powders. . . .	40
3.17	XRD results for atomized Al-0.85%W and Al-1.0%Ta powders. . . .	41

List of Tables

3.1	Polarization Experiments of Al-W alloys	21
3.2	W $4f_{7/2}$ Binding Energies	26
3.3	Calculated Bond Distances about Oxygen	35
3.4	Experimentally Derived Bond Distances about Oxygen	36

EXECUTIVE SUMMARY

Whereas supersaturated aluminum alloys demonstrate enhanced passivity, conventional aluminum alloys spontaneously pit in air-saturated chloride solutions. Under ONR program N00014-85-C-0638, we have investigated the mechanisms involved in several of these alloys. In the 1990 contract year, we have concentrated on three areas: evaluation and characterization of Al-W alloys, which exhibit the best corrosion performance of any alloy system studied to date; characterization of the passive-film structure of Al-Mo alloys; and production and characterization of Al-W and Al-Ta powders, which will be used for compaction into bulk material. Surface analysis of the Al-W passive films formed during polarization show surprising little oxidized solute compared to other alloys. These results indicate that the barrier-layer formation and electrostatic repulsion mechanisms used to explain the passivity of other alloys are not involved here. Instead the W may act to stabilize the passive film structure in a way similar to the way Mo acts in Al-Mo alloys. That is, the oxidized molybdenum reduces the concentration of unstable tetrahedrally coordinated atomic sites, as suggested by reflection extended-x-ray-absorption fine structure (refEXAFS) measurements. Finally, characterization of Al-Ta and Al-W powders indicate that some solute precipitates, but most remains in solid solution. Although such precipitation degrades passivity in cosputter-deposited alloys, the alloys still exhibit superior passivity compared to conventional materials. Characterization of the corrosion behavior of bulk material formed from these powders is ongoing.

1. INTRODUCTION

Aluminum and conventional aluminum alloys are susceptible to localized attack in chloride-containing environments. Although passivity-promoting alloying species, such as Cr and Mo, are commonly added to iron to form corrosion-resistant stainless steels, this approach has traditionally not been applied to aluminum because of the very low solubilities of these alloying additions. As a result, the additions form precipitates that can act as nucleation sites for pitting. Recently, enhanced passivity has been observed in non-equilibrium, supersaturated aluminum alloys formed by sputter deposition,[1-8] ion implantation,[9,10] melt spinning,[11] or physical vapor deposition.[12] For cosputter-deposited alloys containing 6-8 at.% Mo, Cr, Ta, or W, pitting potentials, E_p , range from -200 mV(SCE) to 860 mV(SCE) in 0.1 N KCl, compared with a pitting potential for pure aluminum and its conventional alloys of ~ -690 mV(SCE) (Fig. 1.1). Similar qualitative improvements can also be seen in salt fog tests.

During the 1990 contract year, research on the passivity of supersaturated aluminum alloys proceeded on three fronts: continued investigation of Al-W alloys, production of Al-W and Al-Ta powders for consolidation into bulk material, and evaluation of the structure of Al-Mo passive films. Al-W alloys give the best performance of any alloy system investigated, with E_p 's as high as 1937 mV(SCE) for high concentration (~ 9 at.%) alloys. Using x-ray photoelectron spectroscopy (XPS) to determine the mechanisms behind this enhanced passivity, we have studied the passive film formed at different anodic potentials. Although thin films are ideal for studying the

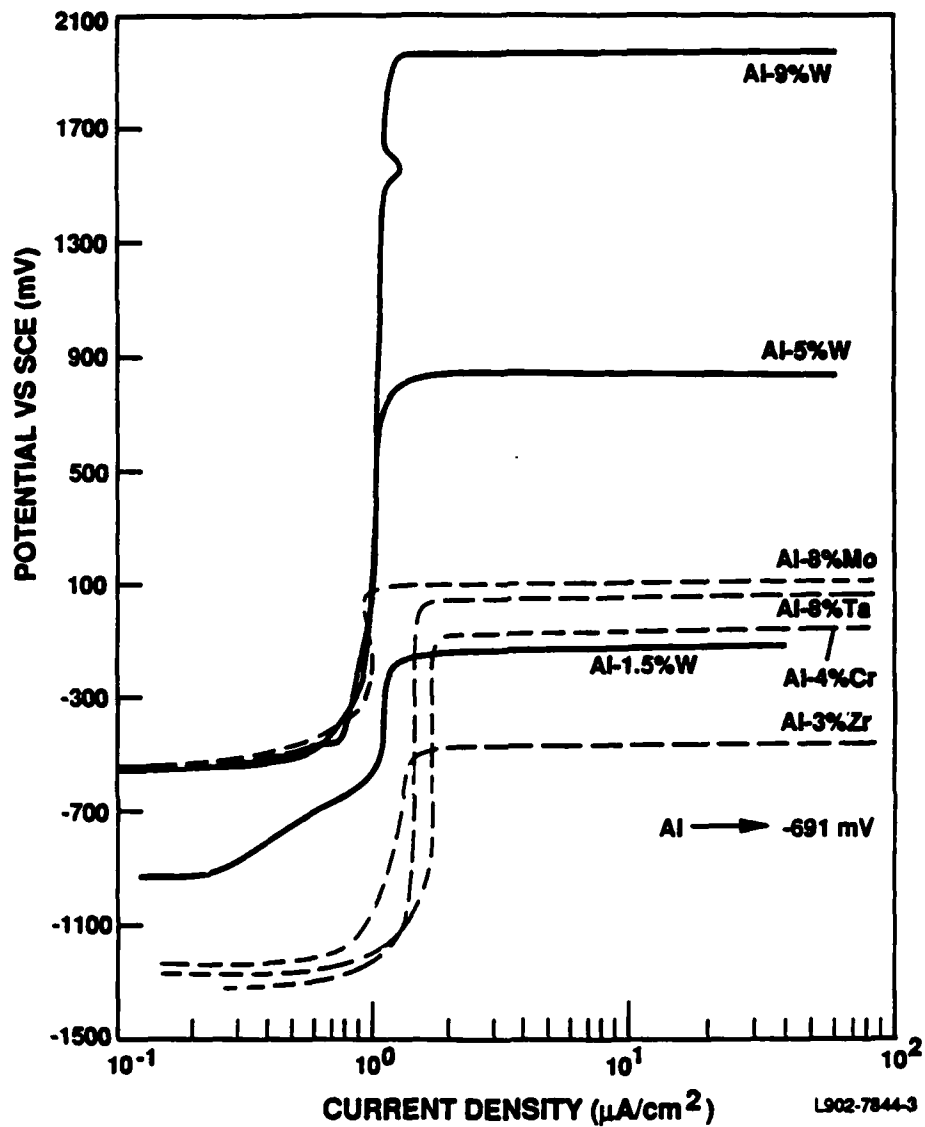


Figure 1.1: Polarization curves for elemental Al and several supersaturated Al alloys in aerated 0.1 N KCl. Data for Al, Al-Zr, Al-Cr, Al-Ta, Al-Mo, and Al-1.5%W represent average or typical results of several specimens; data for the higher concentration Al-W alloys represent results of good, single specimens.

mechanisms of passivity and may be useful in microelectronics, bulk-supersaturated material is needed for most applications. We have chosen dynamic compaction as the means to produce such bulk material and report on the production and characterization of the supersaturated powders. Finally, both the composition and structure of the passive film are likely to govern a material's passivity. For instance, α -Al₂O₃, which contains only octahedral sites is very stable, whereas γ -Al₂O₃, which contains both octahedral and tetrahedral sites, is reactive.[13-15] Accordingly, we have analyzed reflection extended x-ray absorption fine structure spectroscopy (reflEXAFS) results reported earlier[16] on Al-Mo alloys to determine the local structure of their oxide films.

2. EXPERIMENTAL PROCEDURE

2.1 Al-W (Co)sputter-Deposited Alloys

Nine one-micron-thick alloy films were produced by RF magnetron sputter deposition (identical targets) or cosputter deposition (one target Al – the other W) onto Si single-crystal wafers 2-in. (5.08 cm) in diameter. The cosputter deposition process has been described elsewhere.[1-3,5,6] Briefly, this process involves the use of two different target materials with the solute sputtered at a lower power level, typically between 15 and 40 watts, and the Al sputtered at a higher power of approximately 360 watts. Cosputter deposition produces a gradient in solute concentration across the wafers with low solute concentrations on one side of the wafer (the side closest to the Al target) and higher concentrations on the other side (the side closest to the solute target). Cosputter deposition allows a range of compositions, typically several atomic percent difference across the wafer, to be evaluated without having to produce numerous individual wafers. Additionally, cosputter deposition reduces both the number and the cost of the targets needed. Low W concentration alloys were sputtered to a thickness of 2 microns using two identical alloyed targets (Al-1%W) with both of the sputtering guns set at a power level of 400 watts. This process provides uniformity of alloy composition over the surface of the wafer. The Si substrates were kept at 77 K for both deposition processes. Although Frankel[4] has shown that the substrate need not to be cooled in order to exceed the solubility limit for transition metals in Al by a factor of 2 to 3 orders of magnitude, we have continued to deposit our alloys

onto cooled substrates in order to maintain consistency with our earlier work. Solute concentrations for all of the alloys were determined by inductive coupled plasma (ICP). After deposition, the wafers were cleaved into 16 smaller specimens for further evaluation.

Specimen concentration was determined by ICP on wafer sections in the same column of the cosputter-deposited alloys (i.e., the line of specimens equidistant from the two sputter targets) as the tested specimen. This minimized the effect of the composition gradient across the wafer (from column to column) due to varying distances from the two targets. Initial evaluations of the composition gradient across the Al-W alloys seemed to indicate an irregular and wide composition variation.[17] However, analysis, performed on each of the 16 specimens cleaved from one of the wafers, revealed that the W concentration increased from one side of the wafer to the other in a relatively linear fashion. Further investigation indicated that composition values obtained from the corner segments (with approximately one half the area of the remaining segments) were questionable, possibly due to insufficient material. Consequently, all data reported are from specimens whose composition was determined from non-corner segments. The W concentrations across the wafers ranged from a low of ~3% to a high of ~11%. Because the targets used with the sputter-deposited Al-1.5W alloys were identical, no composition gradient was observed; consequently, ICP values were valid across the entire wafer. The W concentrations for these alloys ranged from 1.52 to 1.64% on one wafer and 1.32 to 1.58% on the other wafer.

Alloy composition values were also nondestructively determined from the XPS signal from the substrate (based on the ratio of the alloyed W and metallic Al concentrations).[6] These values tended to be larger than those obtained from ICP, especially for the lower concentration alloys. This difference appears to be real and is likely a result of some W remaining in the alloyed state (instead of dealloying and

forming elemental W – see below) during the preferential oxidation of Al. As a result, the solute concentration near the oxide/metal interface may be greater than that in the bulk.

Glancing angle x-ray diffraction (GXR), [18] with a constant angle of 10 degrees between the incident x-ray beam and the film surface, was used to check each of the alloys for precipitate formation shortly after production and again after long-term storage. The experiments were performed on a Scintag diffractometer using a monochromatic Cu K α x-ray source. The glancing angle was chosen to both optimize the signal from the metal film and prevent diffraction from the Si single-crystal.

Several Al-1.5%W and Al-5%W specimens were vacuum encapsulated and heat treated at 400°C for either 1 or 24 hours to encourage precipitate formation. The thermal stability of the alloys is of interest because the production of bulk metals, one of the goals of this program, may require exposure to elevated temperatures for short periods of time. Following heat treatment, GXR was used to check for precipitate formation and the localized corrosion resistance of these specimens was evaluated using anodic potentiodynamic polarization.

Specimens were masked with Microstop or a marine epoxy paint before immersion in aerated 0.1 M KCl at ambient room temperature (22 to 27°C) and a pH of 7. After the open circuit potential reached steady state (typically within an hour), the specimens were polarized at a scan rate of 0.2 mV/s with a Princeton Applied Research (PAR) Model 273 potentiostat. A limited number of experiments were also run at rates of 0.08 and 0.05 mV/s to confirm that the scan rate was not affecting E_p . All of the electrochemical experiments were conducted on at least duplicate specimens.

The passive-film chemistry was measured by XPS in an iterative procedure on duplicate specimens of each alloy. The as-deposited films were examined first, followed

by the same specimens after they had reached E_{oc} . Finally, after again coming to a steady-state potential, the specimens were polarized to a given potential (500, 800, and 1100 mV above E_{oc}), examined by XPS, repolarized to a higher potential, and again examined by XPS. This procedure continued until E_p was reached. Compositions measured for the E_p specimens are indicative of the passive film rather than the pit itself; the pit's small size prevented its composition from being measured. For the Al-6W alloy, the same specimens were used during the entire procedure; for the Al-1.5W alloy, different specimens were used for the as-received and E_{oc} runs and for the overpotential runs. The use of the same specimens for the Al-6W alloys prevented the compositional gradient across the wafer from complicating the analysis of the evolution of the passive-film chemistry. The Al-1.5W alloys, prepared from binary targets, were much more uniform so that compositional variations were not a factor.

Once the set overpotential or E_p was reached, the specimens were removed from the electrolyte, rinsed in high-purity water, dried with dry nitrogen, cleaned of their masking coating, and inserted into the introduction chamber of the XPS spectrometer. The entire preparation and transportation procedure took less than 6 minutes. Previous evaluations of this transfer procedure indicated no detectable changes in the passive film composition.[2,19] Although the exposure to the ultrahigh vacuum (UHV) will cause any adsorbed water to leave the surface, it will not dehydrate any hydroxides present.

XPS measurements were made using a Surface Science Instruments SSX 100-3 spectrometer having a monochromatized Al $K\alpha$ x-ray source and a hemispherical electron energy analyzer with multichannel detection. The x-ray source was focussed to a spot size of 600 μm ; the take-off angle of the photoelectrons was 52° relative to the surface normal. The surface charge was neutralized by bombardment with low-energy

electrons (~ 2 eV). Binding energies were normalized to adventitious hydrocarbon at 284.8 eV.

Survey spectra were taken to assure no unexpected contamination; high-resolution spectra of the O 1s, C 1s, Al 2p, and W 4f photoelectron peaks were used for quantitative analysis and chemical state determination. Relative concentrations were determined based on peak areas, using an integral background approximation and sensitivity factors derived from standards with our spectrometer. Chemical state separation was obtained by curve fitting the data using the manufacturer's software. To curve fit the W 4f lineshape, the two spin-orbit-split components were constrained by an energy separation of 2.1 eV and an area ratio of 1.33. The criteria for evaluating the fits have been previously published.[3] Chemical state assignments were made using the National Institute of Standards and Technology (NIST) database,[20] supplemented with other sources.[21-27]

2.2 Al-Mo Cosputter-Deposited Alloys

A few days before the reflEXAFS measurements, the Al-Mo specimens were immersed in deaerated 0.1 M KCl (pH 7) and allowed to come to steady state. They were then polarized anodically to -400 mV (SCE). After rinsing in distilled, deionized water and drying, the specimens were placed in a dessicator until the experiments were performed. A witness specimen for each composition was prepared in an identical manner and examined by XPS; the actual reflEXAFS specimens were also examined by XPS following the experiments. For each alloy (7% and 11% Mo), the composition and passive film thickness were unchanged, indicating that the storage, transport, and reflEXAFS measurements did not noticeably affect the specimens.

For comparison, two sputter-deposited pure Al specimens were anodized in 0.2 M tartaric acid neutralized by NaOH to pH 7. The anodization was performed at a constant 7 V for 1200 s to produce a barrier-layer oxide of ~ 10 nm. The same storage, transport, and XPS/reflEXAFS measurement procedures that were described above were followed on these specimens also.

The reflEXAFS measurements were performed at the National Synchrotron Light Source at Brookhaven National Laboratory on the U15 (SUNY/NSLS) beamline which is equipped with a toroidal grating monochromator. A gold mirror was used to direct the monochromated beam toward the experimental station. The soft x-rays entering the sample area impinge first on a gold grid coated with an x-ray-to-visible-light conversion phosphor.[28] The light from this grid serves as the beam monitor (I_0) measurement. The rest of the beam impinges at grazing ($0.5^\circ < \phi < 3.5^\circ$) incidence on the sample, where ϕ is the reflection angle relative to the surface plane. The reflected beam is measured using another phosphor-coated screen. The details of the reflEXAFS analysis are given elsewhere.[16,29]

3. RESULTS AND DISCUSSION

3.1 Sputter-Deposited Al-W Alloys

The alloys were characterized using GXRd shortly after deposition and as a function of time over several months to determine their metallurgical stability. With the exception of several of the higher concentration Al-W alloys, GXRd of all of the cosputter-deposited alloys revealed a highly oriented microstructure with only the {111}, and to a far lesser extent the {311}, planes diffracting the beam. For each specimen, the Al diffraction peak was shifted to higher angles, indicating that smaller W atoms had substitutionally replaced Al in the face-centered-cubic lattice, thereby decreasing the lattice parameter. Glancing angle x-ray diffraction of the sputter-deposited low W concentration alloys (film produced from the binary targets) revealed a more isotropic microstructure with the {111}, {200}, {220}, and {311} planes diffracting the beam. A comparison of the GXRd patterns for pure sputter-deposited Al, a cosputter-deposited Al-7%W alloy and a sputter-deposited Al-1.5%W alloy is presented in Figure 3.1. No evidence of intermetallic phase formation was found in any of the as-sputtered films. Precipitates were observed for both the cosputter-deposited alloys heat treated for 1 hour at 400°C and the sputter-deposited alloys heat treated for either 1 or 24 hours at 400°C. The GXRd patterns for these heat treated specimens are presented in Figure 3.2. In all cases the precipitates were identified as WAl_{12} .

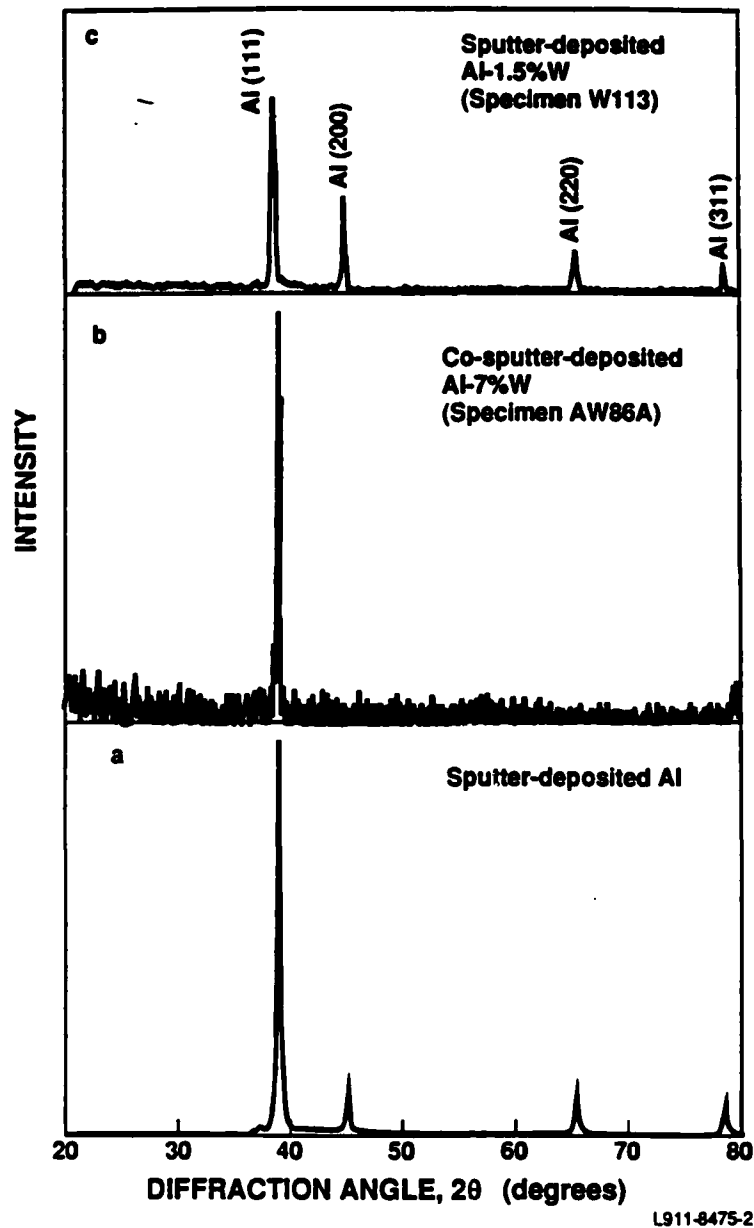


Figure 3.1: Glancing angle x-ray diffraction patterns for sputter-deposited Al (2-micron thick), cosputter-deposited Al-7%W (1-micron thick) and sputter-deposited Al-1.5%W (2-micron thick) alloys. A glancing angle of 10° was used for these measurements and those of Figure 3.2.

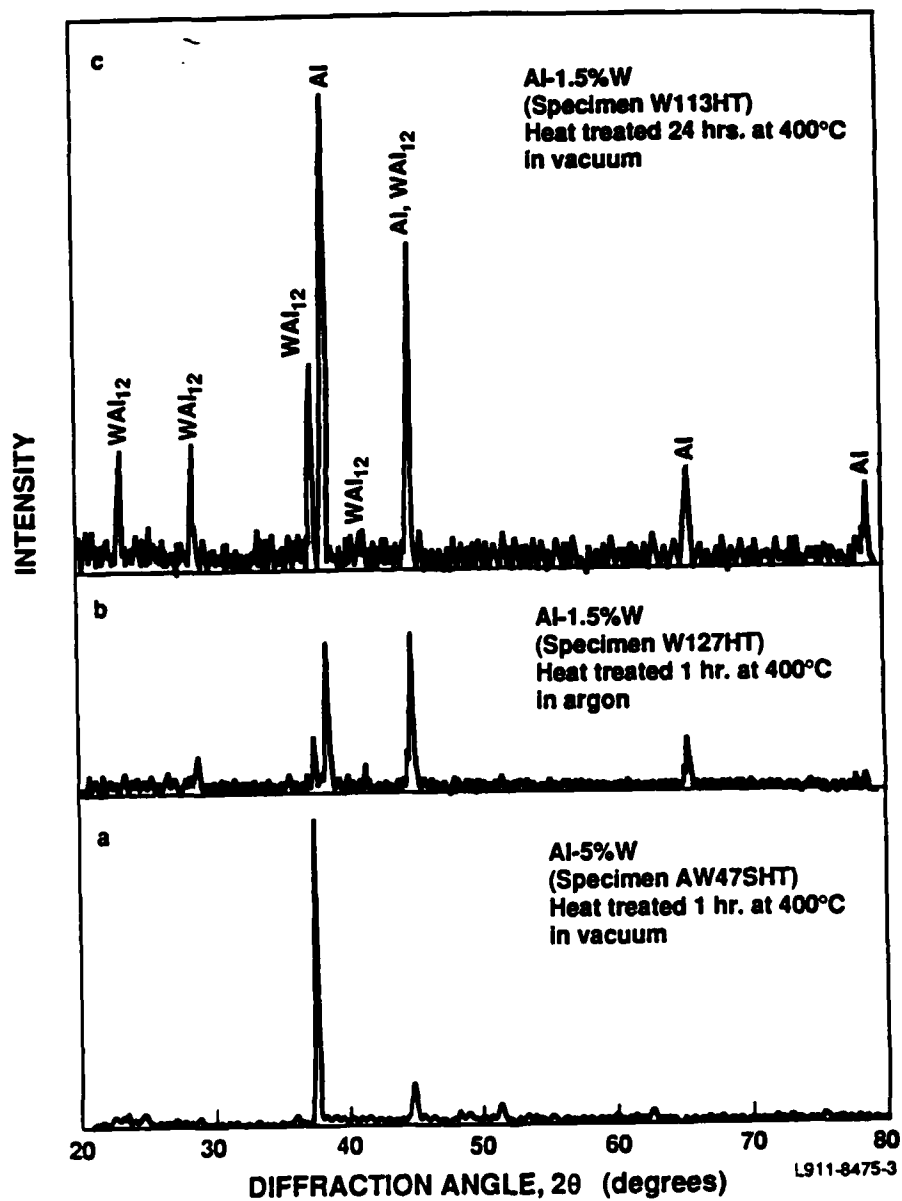
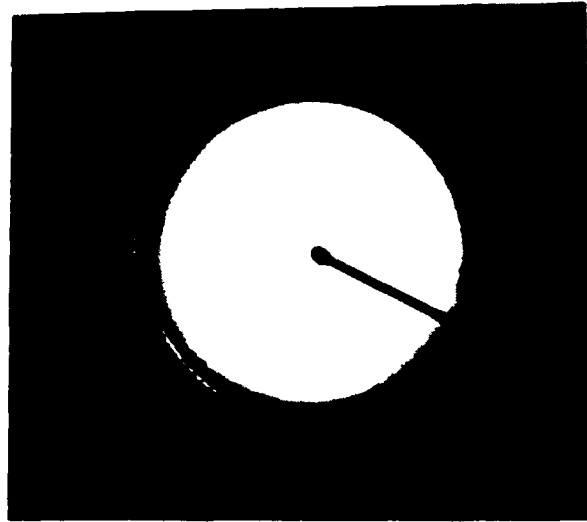


Figure 3.2: Glancing angle x-ray diffraction patterns for a sputter-deposited Al-5%W alloy heat treated at 400°C for 1 hour and sputter-deposited Al-1.5%W alloys heat treated at 400°C for either 1 or 24 hours.

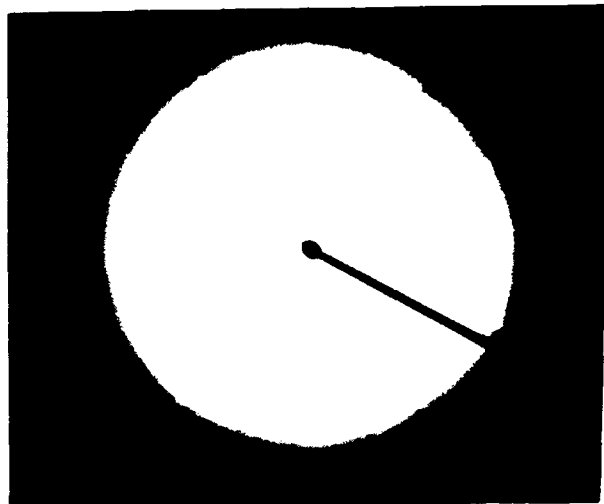
Glancing angle x-ray diffraction of the specimens removed from the far right-hand side of each wafer (highest W concentrations) showed no reflections, which suggests that these alloys were amorphous. Figure 3.3 shows the selected area electron diffraction pattern for one of these specimens and the pattern obtained from a specimen taken from the middle of a wafer, which confirms that the specimens from the far right-hand side of the wafer are amorphous. Similar results have been observed for high concentrations of other transition metals in aluminum.[30] Although the amorphous specimens all had moderate to high W concentrations, no concentration above which all specimens were amorphous and below which all were crystalline was observed. For our specimens amorphousness may be related to both concentration and an increase in the localized cooling rate in this area of the wafer.

Potentiodynamic polarization scans in aerated 0.1 M KCl were generated on 25 specimens taken from various regions of the cosputter-deposited Al-W alloys and on several specimens of the low-concentration sputter-deposited alloys. Tungsten concentrations for these specimens varied from ~ 1 - $\sim 9\%$. The passive current densities were found to be independent of potential within the passive region and similar in value ($1\text{-}2 \mu\text{A}/\text{cm}^2$) to those that we observed for pure Al in deaerated 0.1 M KCl. Specimens with the lowest average solute concentrations exhibited the lowest breakdown potentials and specimens with the highest solute concentrations exhibited E_p values in excess of 1900 mV (Fig. 3.4). The continued sharp increase in E_p with solute concentration is very different from that of the Al-Mo, Al-Cr, and Al-Ta alloys where higher concentration alloys exhibit only small increases in E_p compared to those of moderate-concentration alloys. The E_p values obtained were independent of scan rate within the range of scan rates evaluated (0.2 mV/s to 0.05 mV/s). It was interesting to note that E_p values for the totally amorphous alloys (598 mV and 531 mV) did not differ from those of crystalline alloys with similar compositions. In Fig. 3.5 one of the

Al-W



Crystalline



Amorphous

Figure 3.3: Selected area electron diffraction patterns for Al-W specimens taken from the right-hand side and the center of a cosputter-deposited wafer. The alloy was deposited onto a substrate at 77 K using an Al target power setting of 360 watts and a W target power setting of 40 watts.

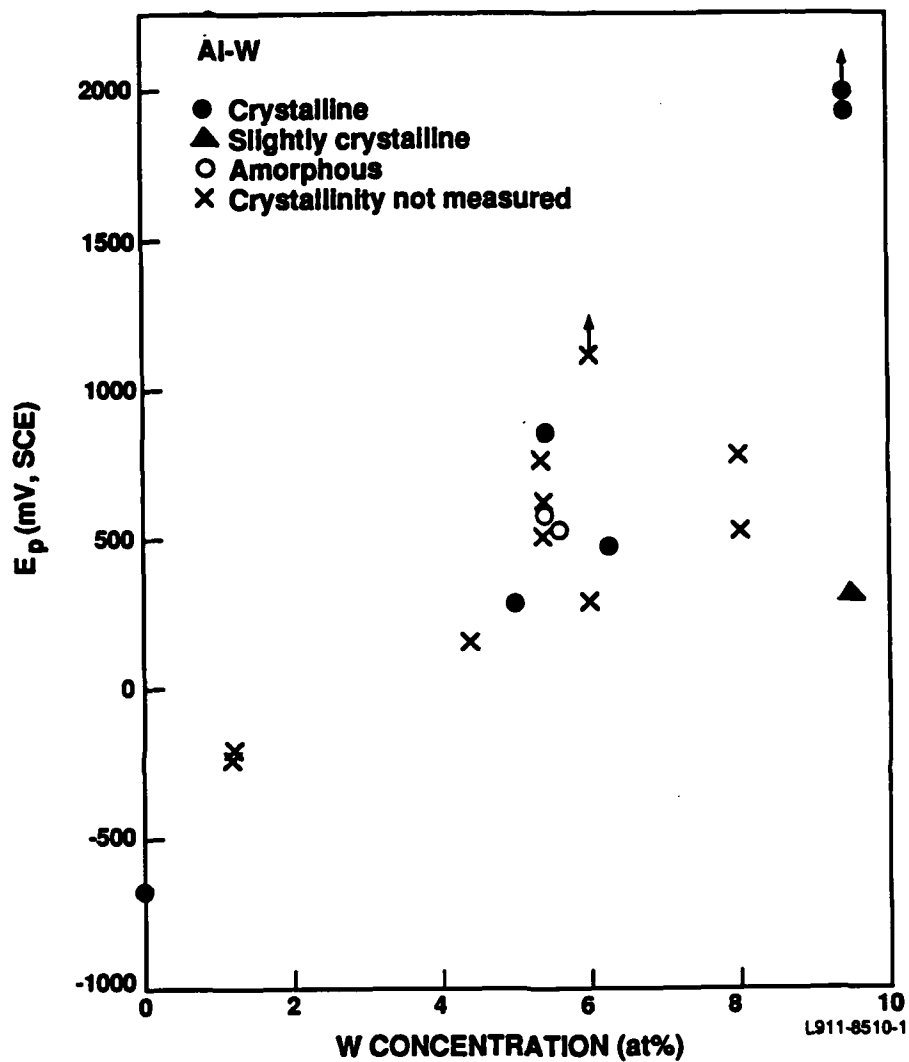


Figure 3.4: Pitting potentials as a function of Al-W alloy concentration. Individual specimens whose crystallinity (or lack thereof) is known are indicated. The majority of the specimens that were not examined by GXR D are assumed crystalline, but all of these are marked unknown.

highest breakdown potentials observed ($\sim 9\%$ W) and an intermediate value of the breakdown potential ($\sim 5\%$ W) can be compared to our earlier results for Al-8%Mo alloys. The polarization behavior of pure W, also shown in this figure, exhibits a high passive current density (on the order of $100 \mu\text{A}/\text{cm}^2$) indicating that W additions enhance the passivity in a potential region in which the pure form does not exhibit a very protective oxide.

Anodic potentiodynamic polarization scans were generated on alloys heat treated at 400°C to determine the effect of precipitates on localized corrosion resistance. Results of these experiments on the cosputter-deposited, higher W concentration specimens heat treated for 1 hour are presented in Figure 3.6. While precipitates clearly degrade the localized corrosion resistance of the Al-W alloys, the performance of these specimens is still equivalent to that of the nonheat-treated Al-8-10%Mo alloys. Heat treatment of the lower W-concentration alloys (1.5%) also resulted in the formation of precipitates. Figure 3.7 reveals that although these precipitates degrade performance, a small passive region, 200 to 300 mV, still remains. Of all the alloys evaluated to date, only the Al-W and the Al-Ta exhibited enhanced corrosion resistance after heat treatment and the resulting nucleation of an intermetallic phase. One possible explanation is that the potential difference between the intermetallic phase and the matrix for these alloys does not promote the formulation of local galvanic cells. However, the potential differences between the intermetallic and the matrix is not known.

Table 3.1 gives the E_{oc} and final potentials for each experimental run. As has been previously observed for Al and Al-Mo, Al-Cr, Al-Zr, and Al-Ta alloys,[3,5] the specimens return to nearly the same E_{oc} at each run, indicating that no significant irreversible changes are occurring during the surface analysis and subsequent storage. The only exception to this observation is the E_{oc} run of specimen 2 of Al-1.5W. The

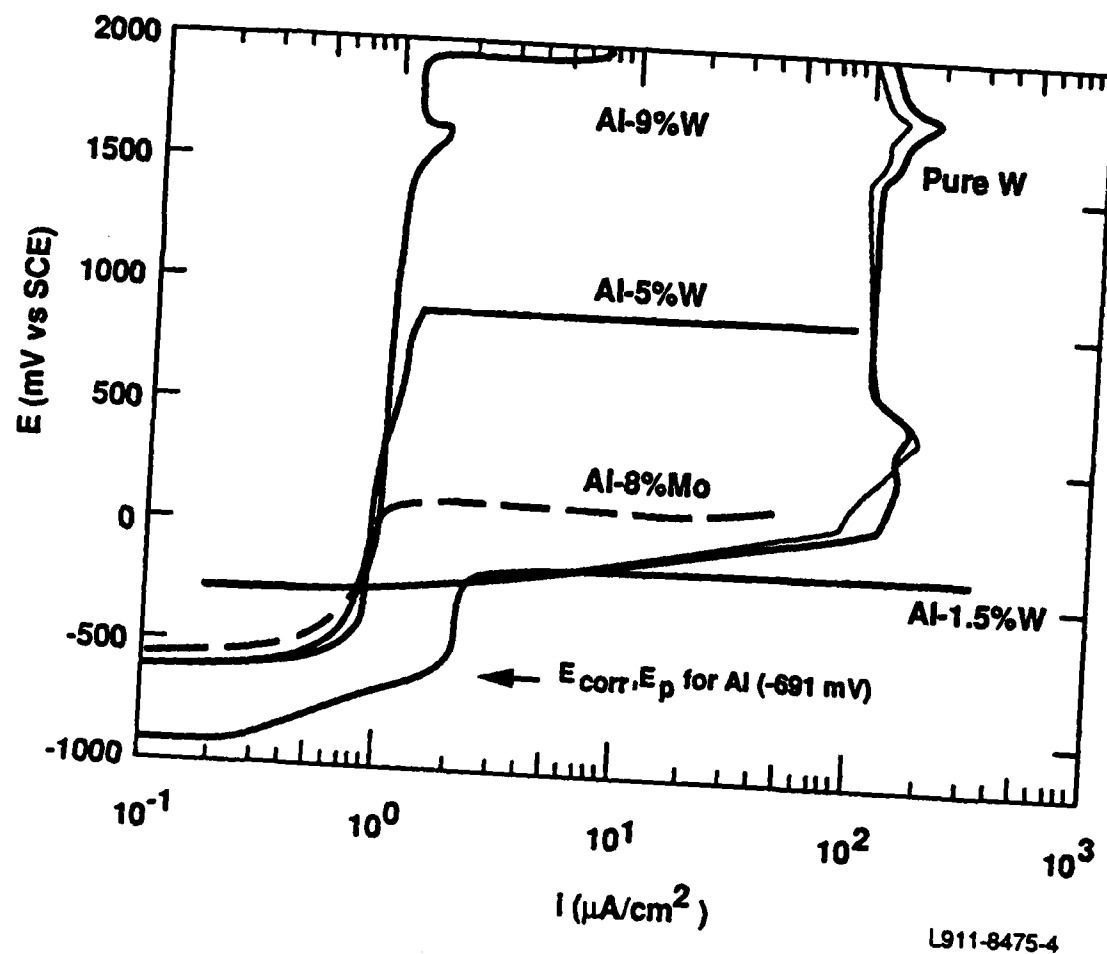


Figure 3.5: Anodic polarization behavior of Al-W alloys in aerated 0.1M KCl (23-25°C) compared to Al-8%Mo (average curve), pure aluminum (average value), and pure W (average curve).

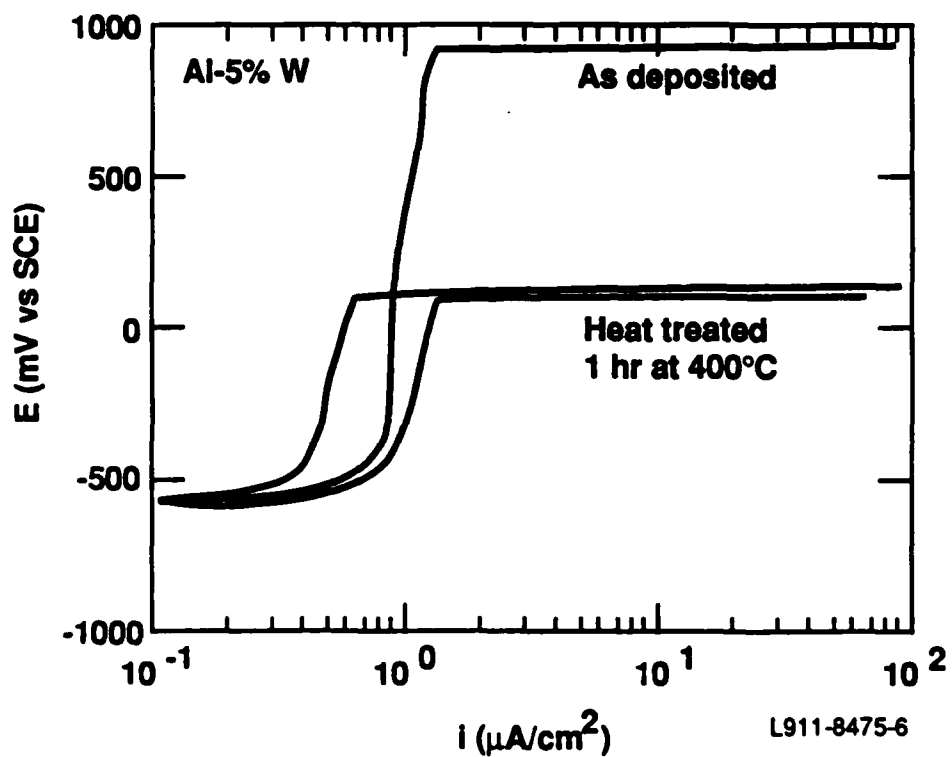


Figure 3.6: Anodic polarization behavior in aerated 0.1M KCl for duplicate Al-5%W specimens heat treated for 1 hour at 400°C compared to a polarization curve for a non-heat treated Al-5%W specimen.

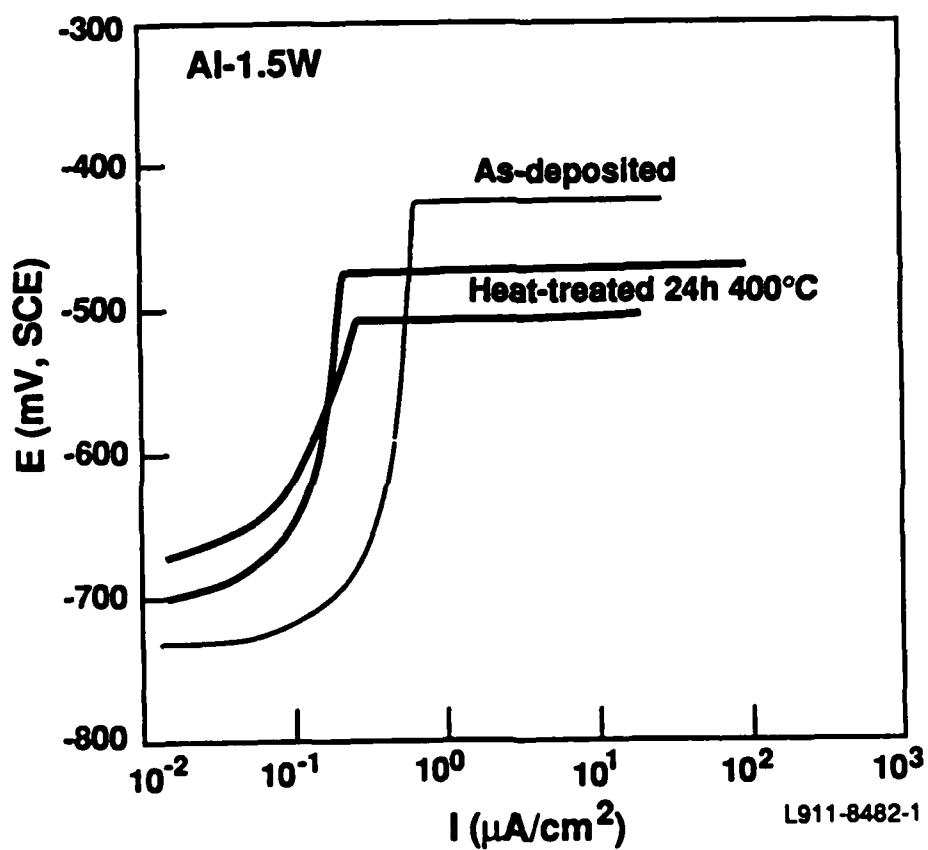


Figure 3.7: Anodic polarization behavior in aerated 0.1 M KCl for Al-1.5%W alloys heat treated at 400°C for either 1 or 24 hours.

Table 3.1: Polarization Experiments of Al-W alloys

run	Al-1.5W		Al-1.5W		Al-6W		Al-6W	
	specimen 1		specimen 2		specimen 1		specimen 2	
	E_{oc}	E_f	E_{oc}	E_f	E_{oc}	E_f	E_{oc}	E_f
	mV	mV	mV	mV	mV	mV	mV	mV
	(SCE)	(SCE)	(SCE)	(SCE)	(SCE)	(SCE)	(SCE)	(SCE)
#1	-895	-895	-705	-705	-635	-635	-640	-640
#2	-848	-348	-879	-379	-623	-123	-617	-117
#3	-874	-212 ^a	-915	-250 ^a	-633	+167	-665	+135
#4					-635	+465	-650	+381 ^a
#5					-653	+483 ^a		

^a E_p

reason for this variation is not known; however, that particular specimen was used only for that run (and as-received). The table clearly shows the improvement in passivity provided by W additions, with increases in E_p of >400 mV for Al-1.5W and >1000 mV for Al-6W compared to pure Al [E_p = -690 mV (SCE)].[7] A weaker dependence of E_{oc} on alloy concentration is also seen, probably because W increases the exchange current density for the reduction reaction.[7]

The evolution of the passive film composition for the two different alloys during polarization is shown in Figures 3.8 and 3.9. Selected XPS spectra as a function of overpotential for one of the Al-6W specimens are presented in Figure 3.10. Several observations can be made from the data: 1) the composition of the passive film is intermediate between $AlOOH$ and $Al(OH)_3$, but closer to $AlOOH$, and remains nearly

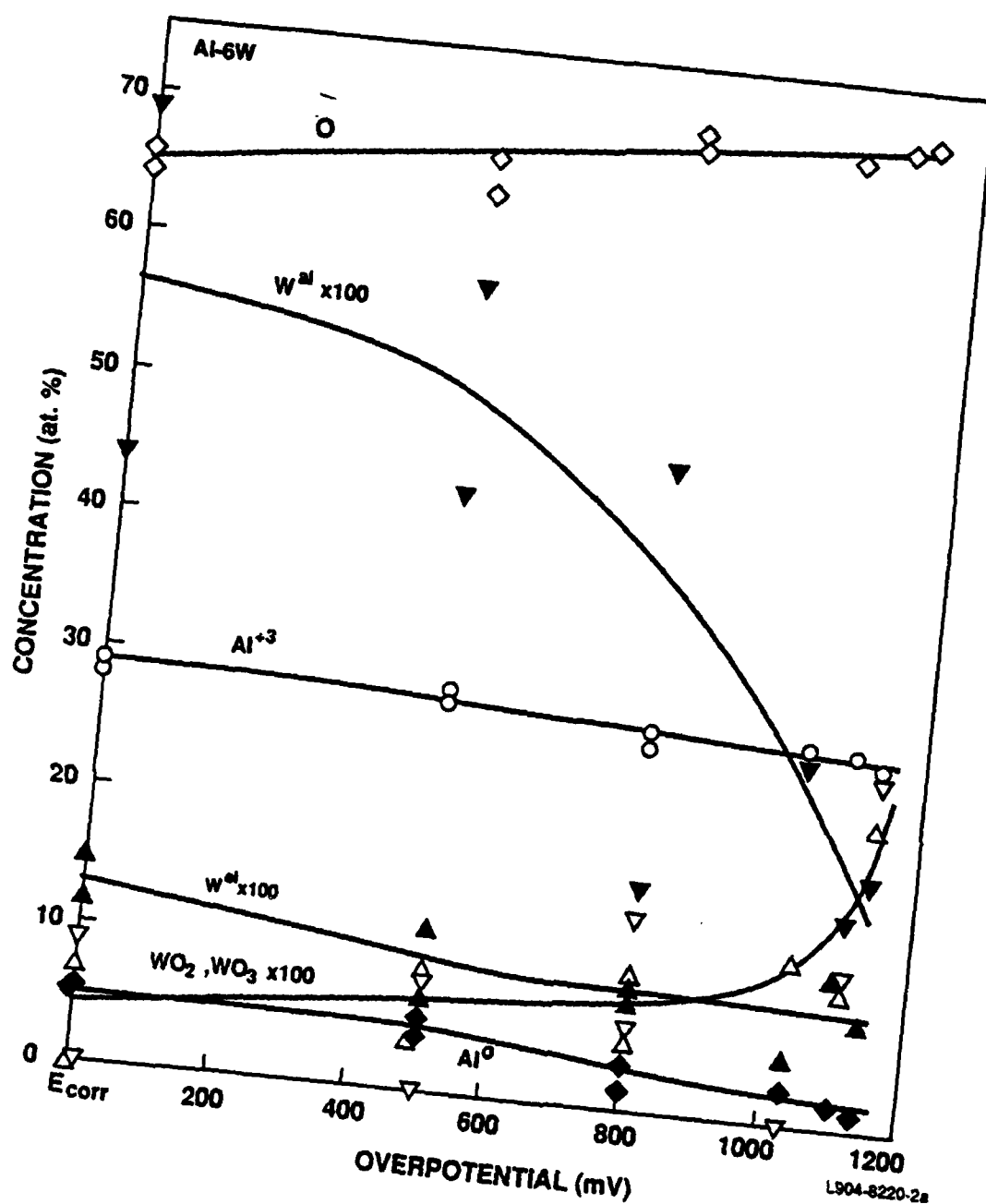


Figure 3.8: Surface composition as measured by XPS for an Al-6W alloy as a function of applied potential: O (\diamond), Al³⁺(\circ), Al⁰(\blacklozenge), WO₃(Δ), WO₂(∇), W^{al}(\blacktriangledown), and W^{el}(\blacktriangle). Note that the concentrations of all W species have been multiplied by 100.

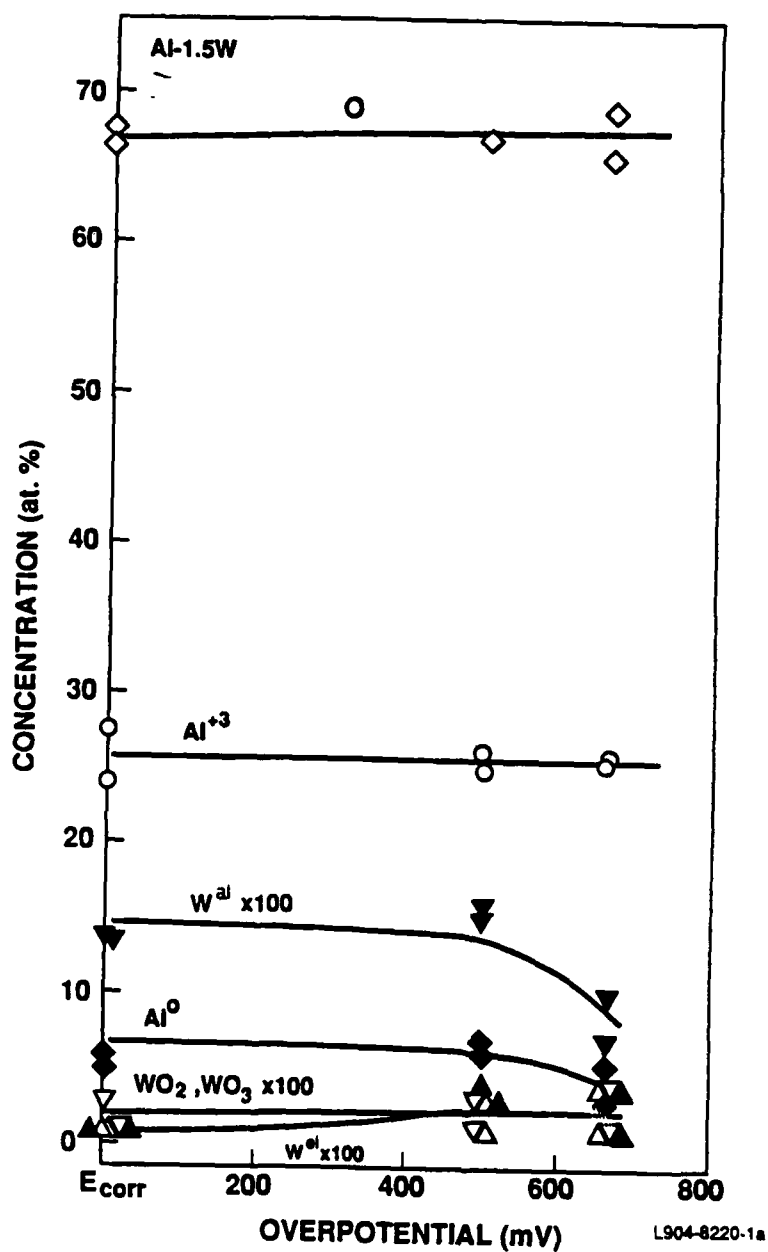


Figure 3.9: Surface composition as measured by XPS for an Al-1.5W alloy as a function of applied potential: O (\diamond), Al^{+3} (\circ), Al^0 (\blacklozenge), WO_3 (\triangle), WO_2 (∇), W^{al} (\blacktriangledown), and W^{el} (\blacktriangle). Note that the concentrations of all W species have been multiplied by 100.

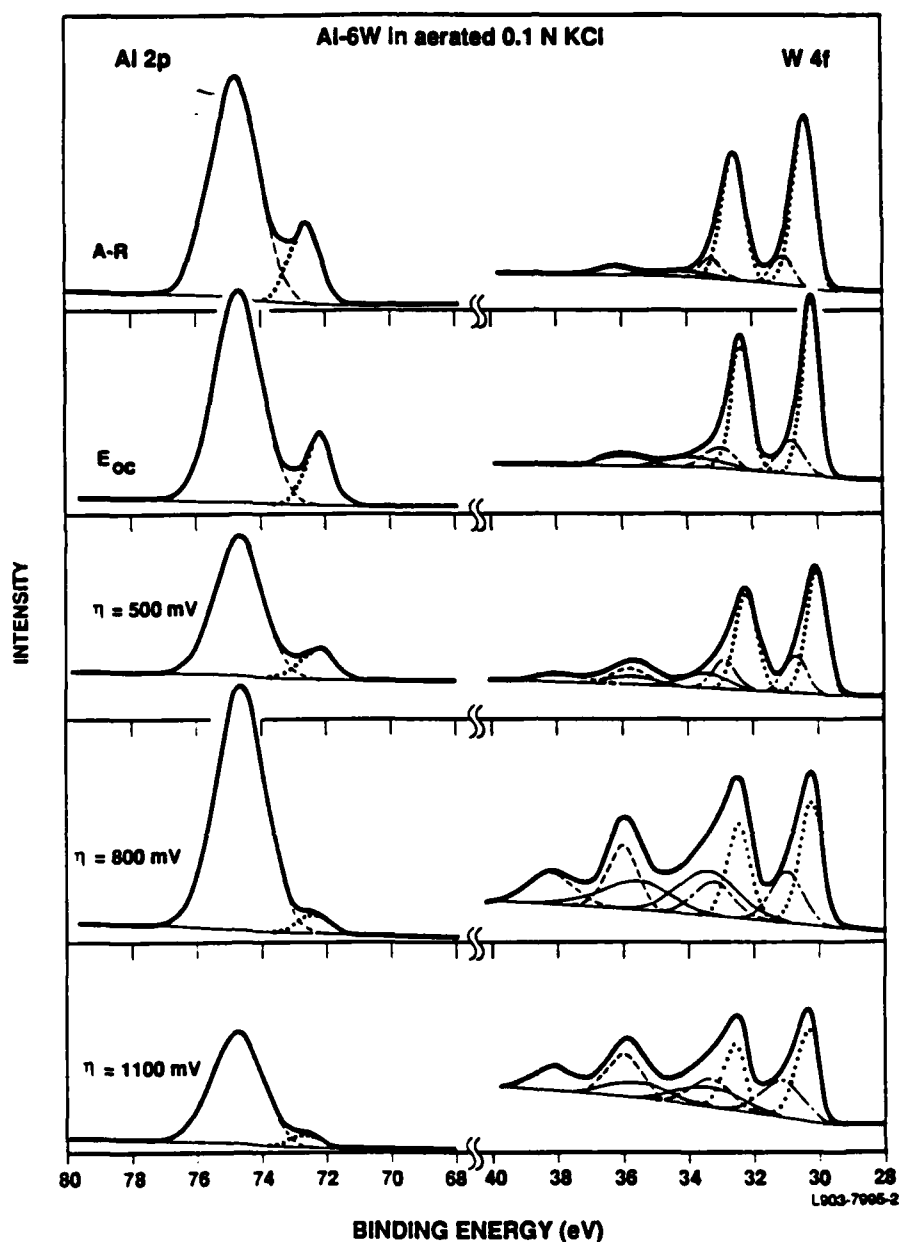


Figure 3.10: Al 2p and W 4f spectra for the Al-6W alloy at different applied potentials. The dotted curves correspond to alloyed W or metallic Al; the dash-dotted curves to elemental W; the thin solid lines to WO_2 ; and the dashed curves to WO_3 and Al^{+3} .

constant; 2) in contrast to the previous alloys investigated, very little solute is found in the passive film, regardless of applied potential; 3) the oxidized W is present as WO_2 and WO_3 (or WO_4^{-2}); 4) the passive film is thin throughout the polarization sequence (ranging from 4 to 6.5 nm); 5) metallic W is also seen in two forms, elemental W (W^{el}) and alloyed W (W^{al}).

A passive-film composition of AlOOH is in agreement with results obtained on pure Al in a variety of electrolytes at near-neutral pH's.[15,19,31,32] It is an intermediate product in the formation of $\text{Al}(\text{OH})_3$, the most thermodynamically stable phase.[33]

The low amounts of oxidized W in the passive films, as shown in Figures 3.8 and 3.9, are surprising in light of the results with the other supersaturated alloys and the superior performance of the Al-W alloys. Oxidized W is typically 0.1-0.2% of the passive film of Al-1.5W alloys and changes little with increasing overpotential. For Al-6W alloys, more oxidized W is found in the oxidized film, ranging from 0.2% to 2% of the oxide/hydroxide, with a general increase at higher potentials, especially near E_p . In marked contrast, passive films of Al-Mo, Al-Cr, Al-Ta, and Al-Zr have considerably more oxidized solute, ranging from ~ 5 -10% for low-concentration Al-Mo alloys up to $\sim 45\%$ for Al-Ta alloys near E_p . [3,5] For these alloys, the oxidized solute concentration depends strongly on overpotential, increasing by a factor of approximately five from E_{oc} to E_p .

The W in the passive film is present as both WO_2 and WO_3 (or WO_4^{-2} ; we cannot distinguish between the two forms of W^{+6}), as the binding energies of Table 3.2 indicate. Because of its low concentration and overlap with other peaks, the binding energy of the state identified as WO_2 was determined with less precision than those of the other states; consequently, its assignment is also based on thermodynamic

Table 3.2: W 4f_{7/2} Binding Energies

Compound	Binding Energy (eV)	
	Alloys	Standards ^a
W ^{al}	30.5	
W ^{el}	31.2	31.3
WO ₂	33.7	32.9
WO ₃	36.1	35.9
WO ₄ ⁻²		35.0-36.3 ^b

^aAverages from Ref. 20.

^bDepends on the cation; Al₂(WO₄)₃: 36.0 eV

considerations. The two oxidized species have nearly equal concentrations, on average, and exhibit identical trends, which were described above.

Like Al-Ta passive films, the ones reported here remained thin even at E_p so that signals from the metallic substrate were readily detectable. We estimate that the film thicknesses ranged from 4 to 6 nm, with the higher-potential films generally thicker than the E_{oc} films. The slow growth of these films differed greatly from that of Al-Mo, Al-Cr, and Al-Zr alloys, which grew so quickly that the substrate could not be detected by XPS following overpotentials of 400-600 mV or higher.

Two metallic W states are detectable – elemental W and a lower-binding-energy state that we identify as alloyed W[3,34] (Table 3.2). As indicated by Figures 3.8 and 3.9, the concentration of W^{al} is proportional to that of metallic Al during the entire polarization sequence. On the other hand, the ratio between the W^{el} and W^{al} concentrations generally increases with increasing overpotential and is very sensitive to

passive film thickness. These results suggest that W^{el} is formed as Al is preferentially oxidized, so that dealloyed (elemental) W is left behind. Indeed, variable-takeoff-angle XPS experiments on \tilde{Al} -Mo alloys, which also exhibit distinct elemental and alloyed solute states, indicate that the elemental state is concentrated at the oxide-substrate interface while the alloyed state is spread throughout the bulk.[3]

For the Al-Mo, Al-Cr, and Al-Ta alloys, we proposed that the enhanced passivity was achieved by oxidized solute (MoO_4^{-2} , $CrOOH$, or Ta_2O_5) which made the passive film more resistant to chloride attack due to electrostatic repulsion or modification of the oxide structure (Al-Mo, see below)[2,3,8] or to barrier layer formation (Al-Cr, Al-Ta).[3,5] In some cases, it also limited the ingress of oxygen into the film. The low concentration of oxidized W coupled with the high passive current density observed for pure W in the neutral pH environment suggests that the electrostatic repulsion and barrier layer mechanisms are not valid here. Instead, the small amounts of oxidized W present in the passive film interact synergistically with the hydrated aluminum oxides to form a more protective passive film in a manner similar to that observed for Cr-Mo and Cr-W combinations in stainless steels.[35-37] It has been postulated that the Mo-Cr and W-Cr combination of stainless steels enhance passivity through either the formation of a more stable oxide layer at the metal-oxide interface or enhanced bonding at the metal-oxide interface. The enhanced resistance to breakdown for the Al-W alloys is likely caused by a reduction in chloride ions penetrating the passive film through to the metallic substrate, which could result from either of the mechanisms suggested above. Not only is chloride ingress restricted for Al-W alloys, but oxygen ingress is restricted even more than it is for Al-Ta alloys. Although the Al-Ta passive film thickness is comparable to that of Al-W, the buildup of Ta_2O_5 in the film and elemental Ta at the passive film-metal interface suggests that the oxidized Al is continually and slowly going into solution and the alloy is oxidizing, leading to a thin

film. For the Al-W alloys, the small buildup of elemental W and its correlation with oxide thickness for Al-W suggest that the passive film is more stable and little Al is being oxidized or dissolved.

3.2 refEXAFS Measurements

Figure 3.11 shows potentiodynamic polarization curves of a comparable Al-Mo specimen, the tartaric-acid-anodized (TAA) pure aluminum specimen, and two unanodized pure aluminum specimens in chloride solutions. Polarization of the Al-Mo specimens to -400 mV(SCE) corresponds to near the middle of their passive region and well above the E_p of pure Al or conventional Al alloys [~ -600 mV(SCE)]. In contrast, anodization in tartaric acid has negligible effect on the pitting potential; the ~ 50 eV increase is likely to be a kinetic effect due to the increased thickness of the oxide and the 0.1 mV/s scan rate of the experiment.

XPS measurements showed the passive film to be 4.0- to 4.5-nm thick and composed predominately of AlOOH with a smaller amount of oxidized Mo as Mo^{+4} as determined by reported binding energies.[3]. Little change in thickness or composition was observed between the witness specimens examined shortly after polarization and the refEXAFS specimens examined upon return from NSLS. These passive films are somewhat thinner than those observed previously for Al-Mo alloys at this potential,[3] but similar in thickness to some of the other supersaturated alloys we have investigated.[5,7,8] Likewise, the passive film contains less oxidized Mo than the previous specimens at this potential, but exhibits comparable chemistry to those of this thickness.

Due to the thinness of the passive film, the near-interfacial region of the substrate

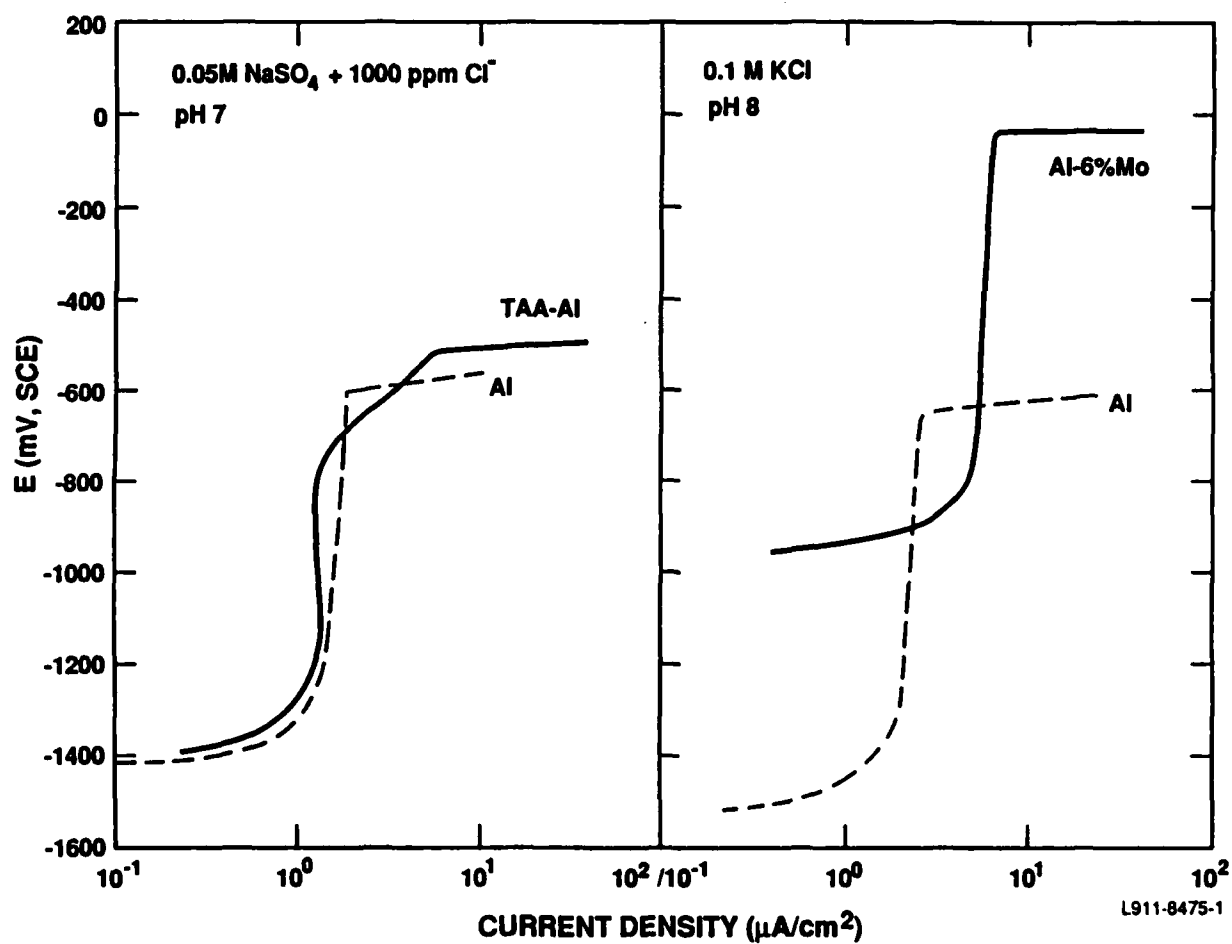


Figure 3.11: Potentiodynamic scans of a) Al-6%Mo and pure Al in 0.1 M KCl and b) TAA Al and unanodized pure Al in 0.05 M Na_2SO_4 with 1000 ppm Cl^-

is also interrogated by XPS. As with other Al-Mo specimens and with Al-Cr and Al-W alloys,[3,7,8] we detect two metallic states – alloyed and elemental Mo. The relative amount of elemental Mo ($\sim 15\%$) corresponds well with that of other alloys at these oxide thicknesses. (As the passive film grows, the fraction of elemental solute at the interface increases until it is the only detectable metallic state just prior to its signal being extinguished itself by the oxide.)

The TAA oxide film was composed of Al_2O_3 and showed no evidence of hydration. As expected from its nominal 10-nm thickness, the substrate was not detectable by XPS.

Reflectivity spectra from the α -alumina (corundum) sample are shown in Figure 3.12. $\chi(k)$ signals were extracted from each of these spectra individually and also from pairs of spectra to solve directly for the optical constants. Consistent with earlier results,[38] it was found that only the $\chi(k)$ data derived from spectra measured below 1.2° yielded mutually consistent results. The magnitude of the Fourier transform of data between $k = 30.4$ and 85.6 nm^{-1} is shown in Figure 3.13. The major peak represents the oxygen-to-aluminum first neighbor distance and the succeeding peaks represent the more distant oxygen-to-oxygen and oxygen-to-aluminum shells.

Reflectivity spectra from surface films on Al-7%Mo, Al-11%Mo, and TAA aluminum differ in character from the corundum data in that there is less high-frequency information in the fine structure. The reflectivity spectra from these surface films were analyzed in the same manner as those from the corundum model compound. As an example, the magnitude of the Fourier transform for data between $k = 29.6$ and 85.6 nm^{-1} is shown in Figure 3.14.

The next step in the analysis is to extract near-neighbor information. Two commonly used methods are comparison of Fourier transform parameters between model

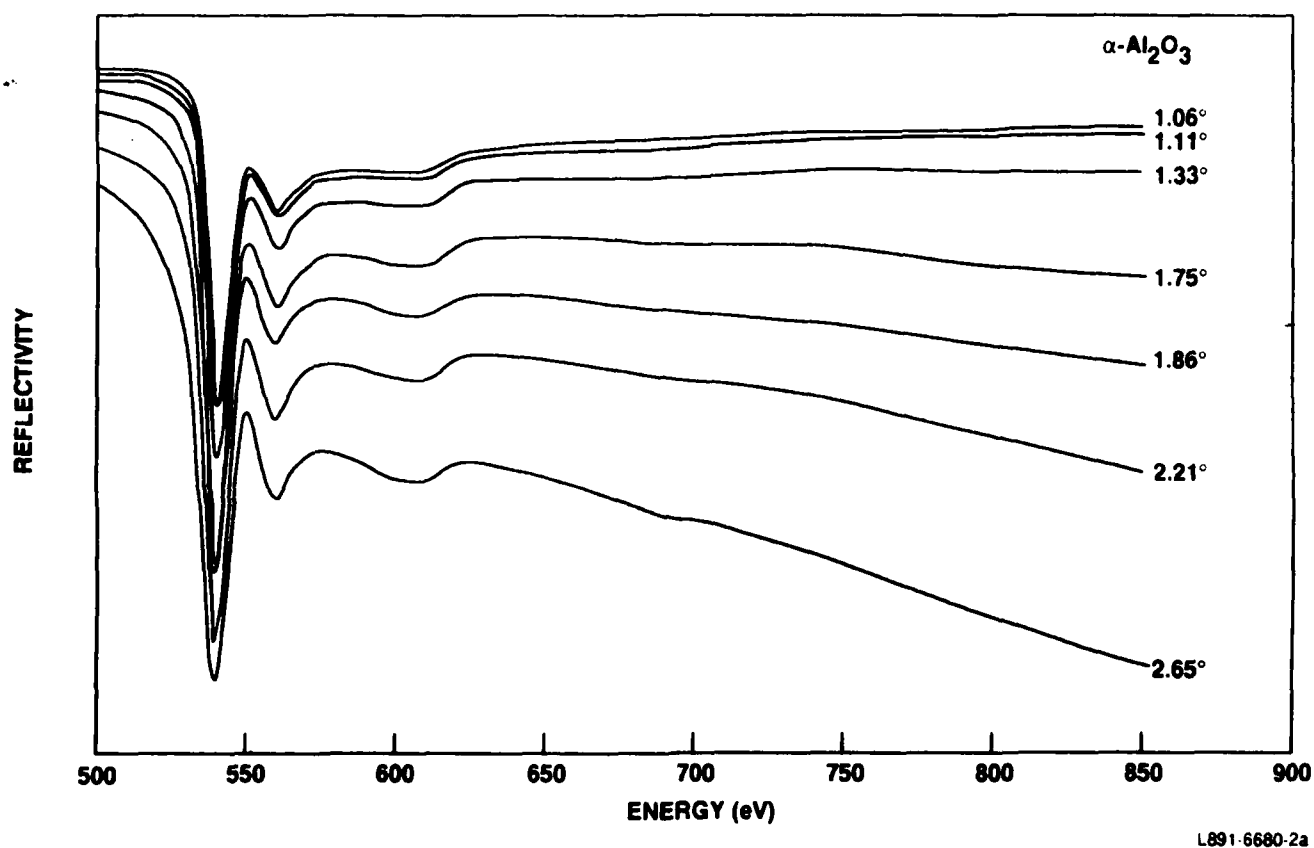


Figure 3.12: Reflectivity spectra measured from single-crystal corundum at seven different reflection angles.

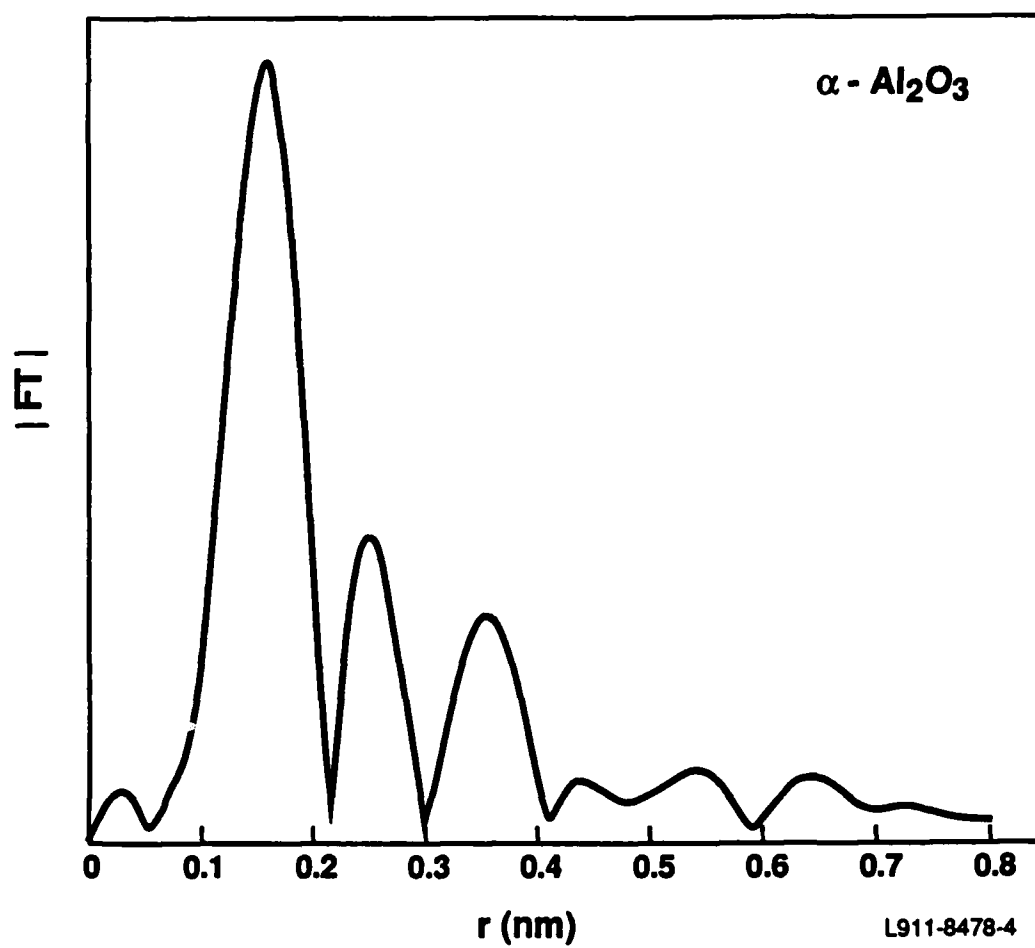


Figure 3.13: Magnitude of the Fourier transform of the reflEXAFS data for corundum, uncorrected for phase.

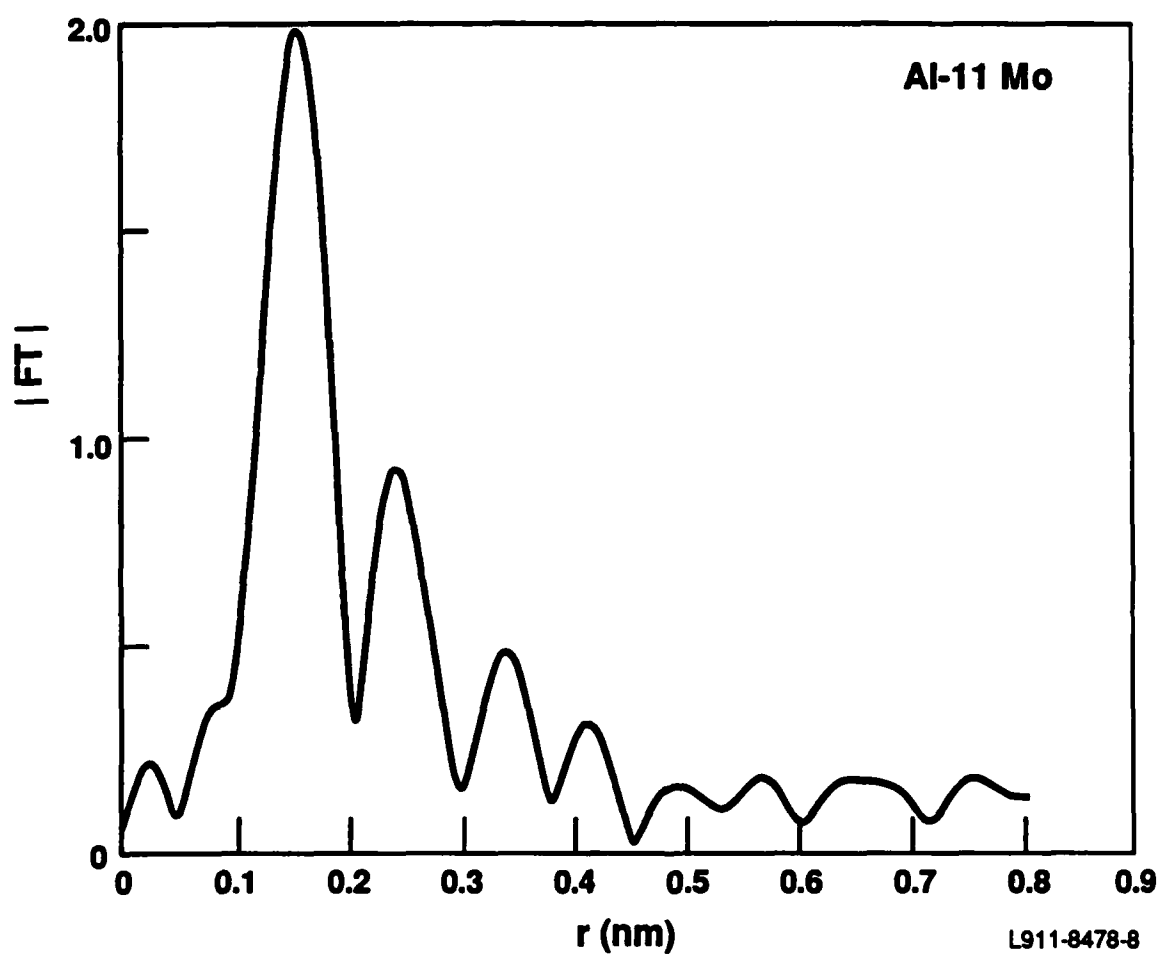


Figure 3.14: Magnitude of the Fourier transform of the data for the passive film on Al-11%Mo, uncorrected for phase.

compounds and the sample and theoretical curve fitting. In the Fourier transform method, the finite length of the data limits the inversion so that many EXAFS studies are made by comparing the unknown system with a known system, i.e., a model compound. The widths and the shapes of the k-space windows are as nearly the same as possible in both cases. The curve-fitting method is often considered to be the preferred method when there is additional information to assist the fitting; however, such data are not available in the present case. Therefore, the analysis of the films formed on Al and on Al-Mo were carried out using the Fourier method and corundum as the model material.

The nearest O-Al and the next nearest O-O neighbors in corundum are shown in Table 3.3. Also shown in the table is the same information for boehmite (AlOOH), gibbsite [$\text{Al}(\text{OH})_3$] and $\gamma\text{-Al}_2\text{O}_3$, some of which are candidate structures for the surface films under investigation here. The $\alpha\text{-Al}_2\text{O}_3$ structure is rhombohedral; the boehmite structure is orthorhombic; the gibbsite structure is monoclinic; and the $\gamma\text{-Al}_2\text{O}_3$ structure is a defect version of a cubic spinel-like structure. In all of these materials, the first neighbor distance is 0.1915 ± 0.003 nm and the number-weighted first-neighbor coordination is 3 or 4. The second neighbor O-O distance varies noticeably among these well-known compounds. Thus, one can reasonably expect to find that the structures in the surface films will vary little in the first near-neighbor distance, and that the coordination number of the first shell would not be a helpful parameter in differentiating among the candidate structures.

The first neighbor distances derived for the Al-7%Mo, Al-11%Mo, and the TAA films are shown in Table 3.4 along with similar results for an air-formed oxide.[39] No second neighbor distance could be derived from the data for the Al-7%Mo film. It can be seen that the structure of the film on the Al-11%Mo is very similar to that of the $\alpha\text{-Al}_2\text{O}_3$ structure (Figs. 3.13 and 3.14). The structure of the surface film on Al-

Table 3.3: Calculated Bond Distances about Oxygen

Structure	$r_1(\text{O-Al})$ (nm)	$r_2(\text{O-O})$ (nm)
$\alpha\text{-Al}_2\text{O}_3$	2 @ 0.1852	2 @ 0.2523
	2 @ 0.1972	2 @ 0.2619
		4 @ 0.2724
		4 @ 0.2861
average	4 @ 0.1912	12 @ 0.2719
$\gamma\text{-Al}_2\text{O}_3$	1 @ 0.1875	3 @ 0.2525
	3 @ 0.1885	6 @ 0.2800
		3 @ 0.3061
	4 @ 1.883	12 @ 0.2797
AlOOH (boehmite)	O_1 4 @ 0.1885	4 @ 0.2498
		1 @ 0.2516
		4 @ 0.2854
		2 @ 0.2868
	O_2 2 @ 0.1908	1 @ 0.2516
		2 @ 0.2689
		4 @ 0.2854
		2 @ 0.2868
	average	3 @ 0.1893
		4 @ 0.2550
		6 @ 0.2859
Al(OH) ₃ (gibbsite)	O_1 1 @ 0.1768 4 @ 0.2.019	1 @ 0.2462
		1 @ 0.2605
		2 @ 0.2721
		1 @ 0.2752
		1 @ 0.2813
		1 @ 0.2991
		1 @ 0.3015
		1 @ 0.3166
		2 @ 0.3209
		1 @ 0.3232
	O_2 2 @ 0.1932	1 @ 0.2514
		1 @ 0.2605
		2 @ 0.2721
		1 @ 0.2813
		1 @ 0.2835
		1 @ 0.2913
		2 @ 0.3157
		2 @ 0.3209
	O_3 1 @ 0.1877 1 @ 0.1946	1 @ 0.2514
		2 @ 0.2723
		1 @ 0.2752
		2 @ 0.2813
		1 @ 0.2913
		1 @ 0.2991
		1 @ 0.3157
		1 @ 0.3166
		1 @ 0.3181
		1 @ 0.3232
	average	3 @ 0.1948
		2 @ 0.2540
		6 @ 0.2820
		4 @ 0.3190

Table 3.4: Experimentally Derived Bond Distances about Oxygen

Specimen	$r_1(\text{O-Al})$ (nm)	$r_2(\text{O-O})$ (nm)
Al-7%Mo	0.185 ± 0.003	—
Al-11%Mo	0.189 ± 0.002	0.268 ± 0.003
TAA Al	0.188 ± 0.002	0.281 ± 0.003
Air-formed native oxide ^a	0.192	0.267

^aRef. 39

7%Mo is apparently a less well ordered version of the film on Al-11%Mo, as evidenced by the difficulties in extracting second neighbor parameters. The parameters derived for the film on the surface of the TAA sample indicate that the structure of this film is more closely related to $\gamma\text{-Al}_2\text{O}_3$ than to $\alpha\text{-Al}_2\text{O}_3$. In contrast, the native oxide film on Al resembles $\alpha\text{-Al}_2\text{O}_3$. [39] It must be noted, however, that a native oxide film is, by definition, formed in the atmosphere and not in solution; immersion in an electrolyte results in the growth of a new passive film [39] that controls the corrosion properties of the specimen.

Using the TAA film as a model for an electrochemically formed oxidized film on Al, the reflEXAFS results suggest that the oxidized Mo stabilizes the passive film by reducing the number of tetrahedral sites. The Al-Mo passive film structure then resembles that of $\alpha\text{-Al}_2\text{O}_3$ instead of that of the more reactive (or less stable) $\gamma\text{-Al}_2\text{O}_3$. Consequently, the passive film on Al-Mo alloys is more able to protect against localized attack than the passive film on pure aluminum or its conventional alloys.

The inherent passivity of the Al-Mo specimens is to be contrasted to apparent

passivity resulting from slowing the kinetics of attack and the particular experimental conditions used to determine E_p . The latter may be useful technologically in extending service lifetimes, but does not change the thermodynamic propensity to pit. As discussed above, we have measured the E_p of these supersaturated aluminum alloys using potentiodynamic polarization at scan rates ranging from 0.05 – 0.2 mV/s and pit initiation tests[19,32] and found little variation in E_p , indicating that the increased passivity is real. On the other hand, thick, homogeneous barrier layer oxide films, such as TAA oxides prepared at higher voltages, will slow the attack of Cl^- irrespective of oxide structure. In these cases, increases in E_p can be observed in potentiodynamic polarizations, depending on scan rate, even though their equilibrium state has not changed.

Combining these refEXAFS results with the electrochemical and XPS results,[7,40] we can infer that the Mo incorporated into the passive film stabilizes it by altering its structure to resemble that of $\alpha\text{-Al}_2\text{O}_3$. The passive film then resists the ingress of Cl^- and prevents localized attack. Only at higher potentials, where the passive film chemistry (and, presumably structure) change with the hydration of the oxidized Mo, does pitting occur.

3.3 Powder Production and Characterization

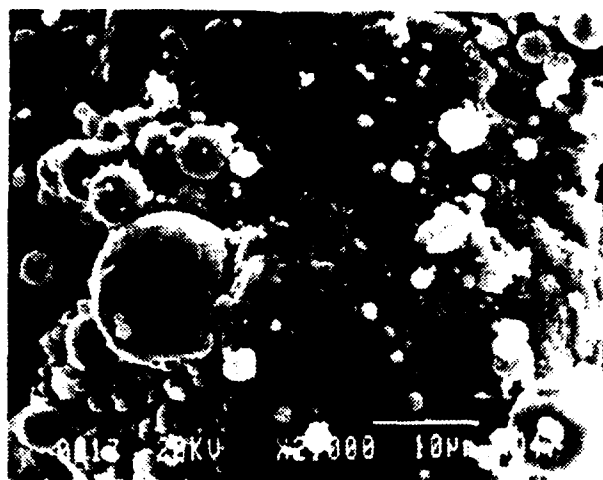
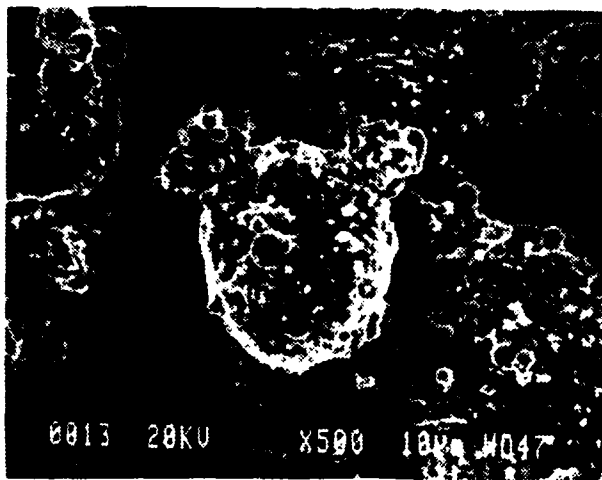
Two batches of atomized powders were produced by Valimet, Inc. The alloys were solutionized at 700-750°C and atomized at 900°C under helium. They were then classified into $< 40\mu\text{m}$, $40 - 75\mu\text{m}$, and $> 75\mu\text{m}$ -diameter particles and packed under argon. Based on the corrosion performance of cosputter-deposited material both as-deposited and after heat treatment to cause precipitation, Al-Ta and Al-W

alloys were chosen as candidates for bulk material. Nominal solute concentrations of 1 at.% were selected as a compromise between corrosion performance and feasibility of powder fabrication and compaction.

The first batch included pure Al, Al-0.56%W, and Al-0.32%Ta. Because the alloy powders had lower concentration than desired, a second batch was prepared of Al-0.85%W and Al-1.0%Ta. The latter were shipped to the Idaho National Engineering Laboratory (INEL) and are being dynamically compacted into bulk material. Samples of both powder batches were sent to Martin Marietta for characterization by SEM and XRD.

Figure 3.15 shows micrographs of the Al, Al-Ta, and Al-W powders from the first batch. The pure Al powders had somewhat irregular shapes and their surfaces had a considerable number of smaller satellite particles. This morphology may make complete compaction more difficult to achieve. In contrast, the Al-Ta and Al-W powders were more spherical in shape and exhibited much fewer satellite particles. The presence of small precipitates can be seen on the surface of the Al-W powders and is indicated by the XRD results of Figure 3.16. As we showed above, although precipitation degrades the corrosion performance of Al-W alloys, they still demonstrate passivity in air-saturated KCl solutions. Nonetheless, the precipitates found here are different from the WAl_{12} precipitates seen in the (co)sputtered-deposited films and the effect of the former on the passivity will need to be determined. On the other hand, no precipitates were detected in the Al-0.32%Ta powders.

Similar particle morphology was seen for the second batch of alloy powders - nearly spherical shapes with a few satellite particles. X-ray diffraction indicates that the higher alloy concentration results in precipitation in both the Al-Ta and Al-W alloys (Fig. 3.17). The precipitation in the Al-Ta powders was investigated as



Al-W PPTs

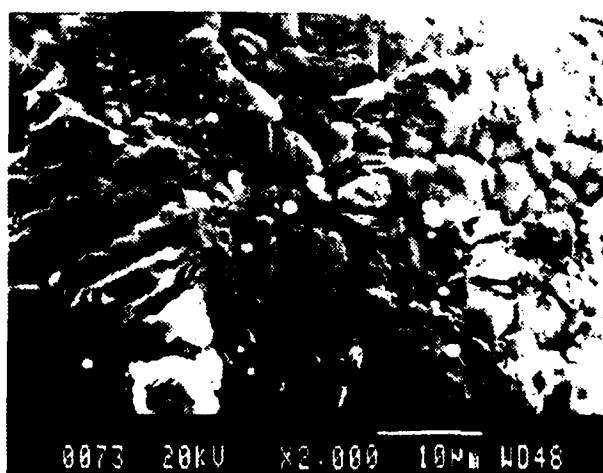
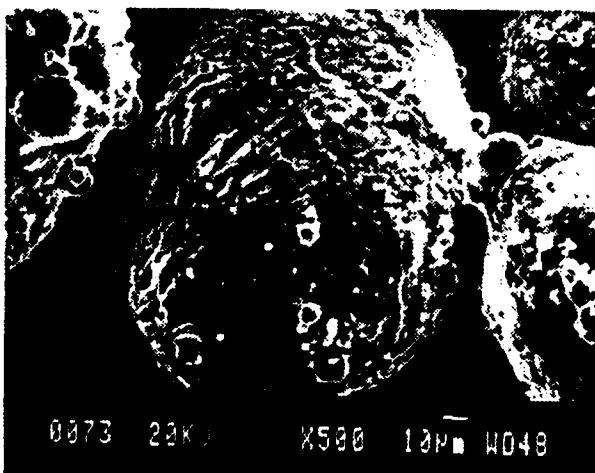
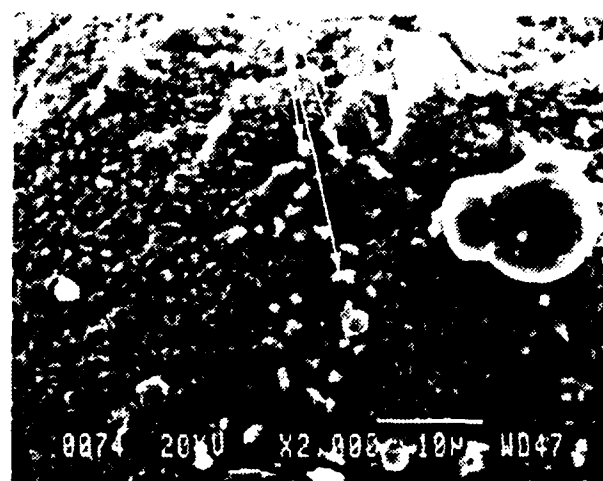
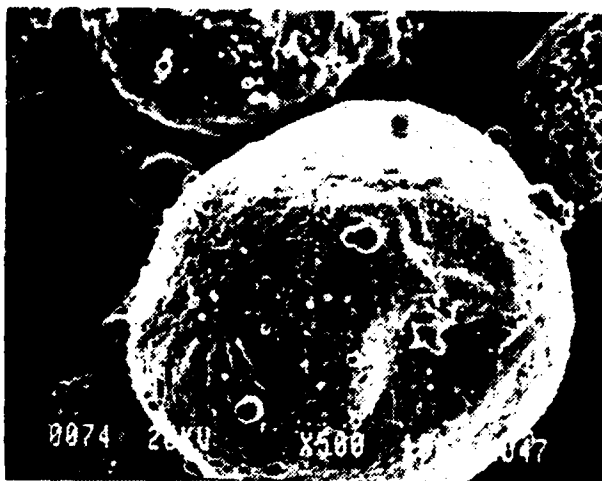


Figure 3.15: SEM micrographs of atomized Al, Al-0.56%W, and Al-0.32%Ta powders.

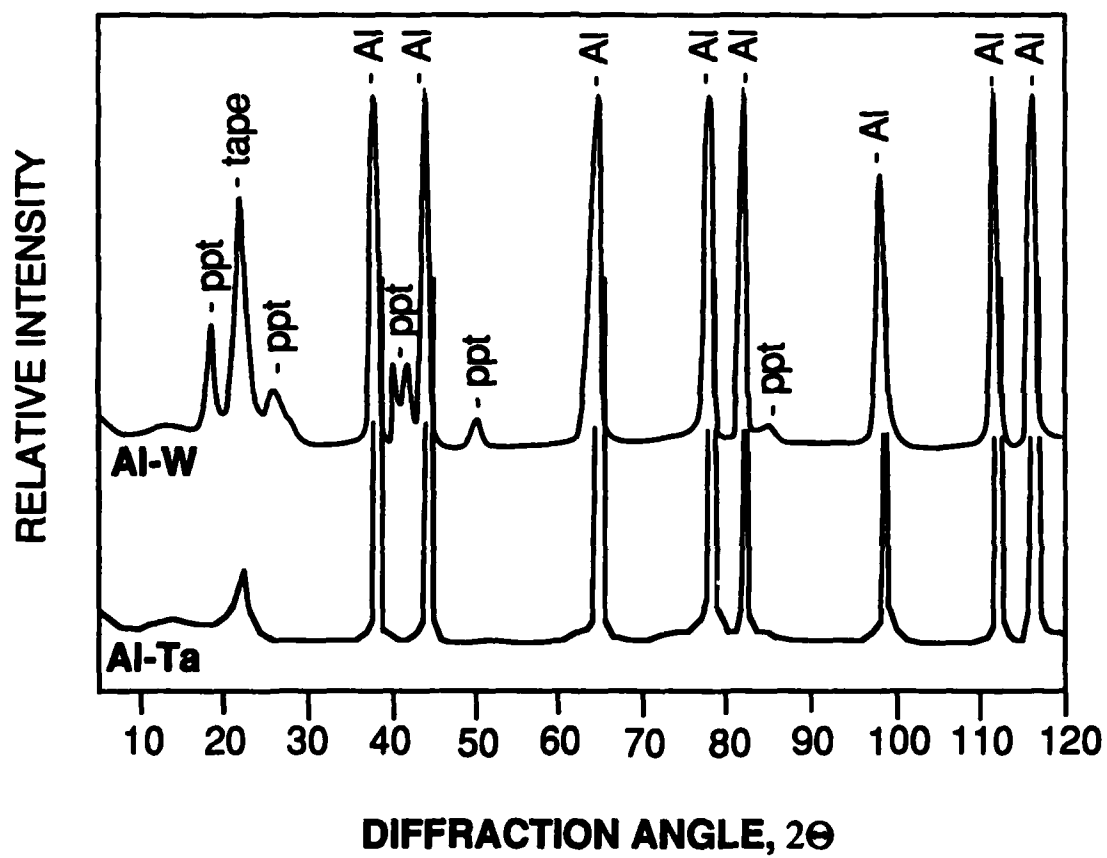


Figure 3.16: XRD results for atomized Al-0.56%W and Al-0.32%Ta powders.

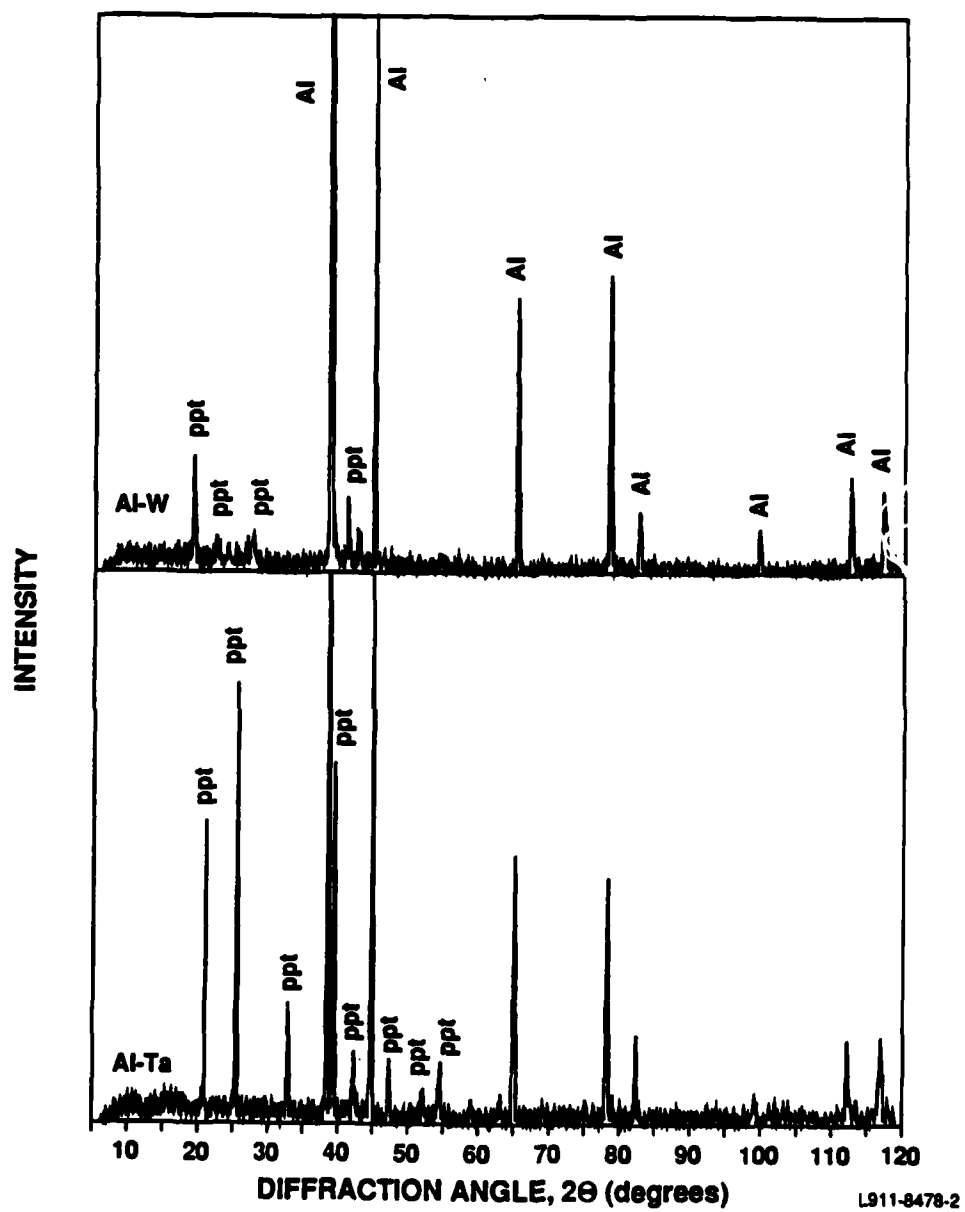


Figure 3.17: XRD results for atomized Al-0.85%W and Al-1.0%Ta powders.

a function of powder size to see if smaller particles with their greater cooling rate would be homogeneous. All powders down to 10-30 μm in diameter (the practical limit of compaction[2,3]) showed the presence of Al_3Ta precipitates, but at decreasing concentration in the smaller sized particles. Again, previous results with cosputter-deposited films suggested continued passivity with heat treatment of Al-Ta alloys; nonetheless, compaction will be attempted with the finer particles to minimize the second phase.

4. SUMMARY AND CONCLUSIONS

Based on the electrochemical, material, and surface characterizations discussed above, the following conclusions can be drawn:

1. The most dramatic improvements in passivity that we have observed to date for nonequilibrium alloys have been for the Al-W alloys.
2. Long term (greater than 1 year) room-temperature storage of the Al-W alloys, like that of all of the alloys we have examined to date (with the exception of Cu) does not result in the precipitation of a second phase, which could be detrimental to corrosion resistance.
3. Tungsten concentrations of approximately 6% or more combined with very rapid cooling rates can lead to the formation of amorphous alloys.
4. Alloy grain size may play a role in enhancing passivity. A correlation between enhanced passivity and alloy grain size was observed where the alloys with the smallest grains exhibited the best corrosion performance. However, amorphous and crystalline specimens of the same compositions exhibited similar passivities.
5. In the crystalline material, the addition of approximately 9% W to Al results in positive shifts in E_p of as much as 2600 mV. At low W concentrations (1.5%), E_p for the alloys is shifted 500 mV over that of pure Al.
6. Al-W alloys heat treated at 400°C form a second phase that has been identified

as WAl_{12} . The localized corrosion resistance of the heat-treated alloys is less than that of the one phase alloys, but performance of the heat-treated higher W concentration alloys is still comparable to that observed for the non-heat-treated Al-Mo and Al-Cr alloys of approximately the same solute concentration.

7. The mechanism of passivity enhancement for the Al-W alloys is neither the barrier-layer formation observed for Al-Ta and Al-Cr alloys nor the electrostatic repulsion mechanism contributing to the passivity of Al-Mo alloys; instead the small amount of oxidized W in the Al-W passive film must somehow synergistically interact with the aluminum oxides in the film to form a more protective or stable passive film.

8. The passivity of the Al-Mo alloys also involves a stabilization of the oxide structure through the reduction of tetrahedrally coordinated sites in favor of octahedrally coordinated sites. The resulting structure, although amorphous, resembles that of stable $\alpha-Al_2O_3$. Only as the molybdate in the film hydrates, with a presumed structure change, does the alloy pit. A similar mechanism may also provide the passivity of the Al-W alloys.

9. Atomized powders of low-concentration Al-W and Al-Ta alloys can be produced albeit with some precipitation. Results with cosputter-deposited Al-W and Al-Ta alloys that have been heat-treated indicate that passivity is maintained (at a lower level) despite the presence of precipitates. These powders will undergo dynamic compaction and the bulk material will be evaluated during the current contract year.

ACKNOWLEDGEMENTS

We gratefully acknowledge K.A. Olver for assisting with the x-ray photoelectron spectroscopy. We would like to thank G. S. Frankel and M.A Russak of the IBM Research Division - T.J. Watson Research Center for their helpful discussions concerning highly alloyed Al thin films. This program was funded by A.J. Sedriks of the Office of Naval Research under contract no. N00014-85-C-0638.

5. REFERENCES

- [1] W.C. Moshier, G.D. Davis, J.S. Ahearn, and H.F. Hough, *J. Electrochem. Soc.* **133**, 1063 (1986).
- [2] W.C. Moshier, G.D. Davis, J.S. Ahearn, and H.F. Hough, *J. Electrochem. Soc.* **134**, 2677 (1987).
- [3] W.C. Moshier, G.D. Davis, and G.O. Cote, *J. Electrochem. Soc.* **136**, 356 (1989).
- [4] G.S. Frankel, M.A. Russak, C.V. Jahnes, M. Miramaani, and V.A. Brusic, *J. Electrochem. Soc.* **136**, 1243 (1989).
- [5] G.D. Davis, W.C. Moshier, T.L. Fritz, and G.O. Cote, *J. Electrochem. Soc.* **137**, 422 (1990).
- [6] B.A. Shaw, T.L. Fritz, G.D. Davis, and W.C. Moshier, *J. Electrochem. Soc.* **137**, 1317 (1990).
- [7] B.A. Shaw, G.D. Davis, T.L. Fritz, B.J. Rees, and W.C. Moshier (submitted to *J. Electrochem. Soc.*).
- [8] G.D. Davis, T.L. Fritz, K.A. Olver, B.J. Rees, B.A. Shaw, and W.C. Moshier, in *Proc. Symp. Applications of Surface Analysis Methods to Environmental/Materials Interactions*, D.R. Baer, C.R. Clayton, and G.D. Davis, eds., (Electrochemical Society, Pennington, NJ, 1991) (in press).
- [9] P.M. Natishan, E. McCafferty, and G.K. Hubler, *J. Electrochem. Soc.* **133**, 1061 (1986).

- [10] P.M. Natishan, E. McCafferty, and G.K. Hubler, J. Electrochem. Soc. **135**, 321 (1988).
- [11] H. Yoshioka, S. Yoshida, A. Kawashima, K. Asami, and K. Hashimoto, Corros. Sci. **26**, 795 (1986).
- [12] R.W. Gardiner and M.C. McConnell, Metals Mater. **3**, 254 (1987).
- [13] G. Ervin, Jr., Acta Crystal. **5**, 103 (1952).
- [14] B.C. Lippens and J.H. de Boer, Acta Cryst. **17**, 1312 (1964).
- [15] R.S. Alwitt, *Oxides and Oxide Films*, Vol. 4 (Marcel Dekker, New York, 1975), p. 169.
- [16] G.D. Davis, W.C. Moshier, T.L. Fritz, G.O. Cote, G.G. Long, and D.R. Black, "Evolution of the Chemistry of Passive Films of Sputter-Deposited, Supersaturated Al Alloys," MML TR 89-12c, Annual Report for ONR Contract N00014-85-C-0638 (January 1989).
- [17] B.A. Shaw, G.D. Davis, T.L. Fritz, and W.C. Moshier, "A Study of the Influence of Alloying Additions on the Passivity of Aluminum," MML TR 90-28c, Annual Report for ONR Contract N00014-85-C-0638 (February 1990).
- [18] M. Nathan, Mater. Lett. **3**, 319 (1985).
- [19] G.D. Davis, W.C. Moshier, J.S. Ahearn, H.F. Hough, and G.O. Cote, J. Vac. Sci. Technol. A **5**, 1152 (1987).
- [20] C.D. Wagner and D.M. Bickham, NIST Standard Reference Database 20, NIST X-ray Photoelectron Spectroscopy Database, Version 1.0, National Institute of Standards and Technology, Gaithersburg, MD (1989).

- [21] C.D. Wagner, W.M. Riggs, L.E. Davis, J.F. Moulder, and G.E. Muilenberg, eds., *Handbook of X-ray Photoelectron Spectroscopy* (Perkin-Elmer, Eden Prairie, MN 1979).
- [22] C.D. Wagner, in *Practical Surface Analysis*, eds., D. Briggs and M.P. Seah (Wiley, Chichester, 1983), p. 477.
- [23] G.E. McGuire, G.K. Schweitzer, and T.A. Carlson, *Inorg. Chem.* **12**, 2450 (1973).
- [24] K.T. Ng and D.M. Hercules, *J. Phys. Chem.* **80**, 2094 (1976).
- [25] R.J. Colton and J.W. Rabalais, *Inorg. Chem.* **15**, 236 (1976).
- [26] P. Biloen and G.T. Pott, *J. Catal.* **30**, 169 (1973).
- [27] J.F. Morar, F.J. Himpsel, G. Hughes, J.L. Jordan, F.R. McFeely, and G. Hollinger, *J. Vac. Sci. Technol. A* **3**, 1477 (1985).
- [28] B.X. Yang, J. Kirz, and S. Xu, *Nucl. Instrum. Meth.* **A258**, 141 (1987).
- [29] G.D. Davis, W.C. Moshier, G.G. Long, and D.R. Black (submitted to *J. Electrochem. Soc.*)
- [30] G.S. Frankel, IBM Research Division – T.J. Watson Research Center, (personal communication).
- [31] W. Vedder and D.A. Vermilyea, *Trans. Faraday Soc.* **65**, 561 (1969).
- [32] W.C. Moshier, G.D. Davis, and J.S. Ahearn, *Corros. Sci.* **27**, 785 (1987).
- [33] E. Deltombe, C. Vanleughenaghe, and M. Pourbaix, *Atlas of Electrochemical Equilibria in Aqueous Solutions* (Pergamon Press, Oxford, 1966), p. 168.
- [34] W.F. Egelhoff, *Surf. Sci. Rep.* **6**, 253 (1986).

- [35] A.E. Yaniv, J.B. Lumsden, and R.W. Staehle, *J. Electrochem. Soc.* **124**, 490 (1977).
- [36] I. Olefjord, *Mater. Sci. Engr.* **42**, 161 (1980).
- [37] N. Bui, A. Irhzo, F. Dabosi, and Y. Limouzin-Maire, *Corrosion* **39**, 491 (1983).
- [38] G.G. Long, J. Kruger, D.K. Tanaka, and Z. Zhang (in preparation).
- [39] J. Stöhr, D. Denley, and P. Perfetti, *Phys. Rev. B* **18**, 4132 (1978).
- [40] W.C. Moshier, Martin Marietta Space Systems, (unpublished).
- [41] G.E. Korth, Idaho National Engineering Laboratory, (personal communication)

6. PUBLICATIONS DURING THE 1990 CONTRACT YEAR

G.D. Davis, W.C. Moshier, T.L. Fritz, and G.O. Cote, "Evolution of the chemistry of passive films of sputter-deposited, supersaturated Al alloys," *J. Electrochem. Soc.* **137**, 422 (1990).

B.A. Shaw, T.L. Fritz, G.D. Davis, and W.C. Moshier, "The influence of tungsten on the pitting of aluminum films," *J. Electrochem. Soc.* **137**, 1317 (1990).

D.R. Baer, C.R. Clayton, and G.D. Davis, eds., *Proc. Symp. Applications of Surface Analysis Methods to Environmental/Materials Interactions*, (Electrochemical Society, Pennington, NJ, 1991) (in press).

G.D. Davis, T.L. Fritz, K.A. Olver, B.J. Rees, B.A. Shaw, and W.C. Moshier, "Passivity enhancement of aluminum with tungsten alloying additions," (*ibid.*)

7. PRESENTATIONS DURING THE 1990 CONTRACT YEAR

“Alloying Additions for Enhancing the Localized Corrosion Resistance of Aluminum,” B.A. Shaw, G.D. Davis, T.L. Fritz, K.A. Olver, and W.C. Moshier, Symp. on Practical Applications of Electrochemical Corrosion Techniques (Baltimore, MD, Dec. 1989).

“Passivity Enhancement of Aluminum with Tungsten Alloying Additions,” G.D. Davis, T.L. Fritz, K.A. Olver, B.J. Rees, B.A. Shaw, and W.C. Moshier, 178th Meeting Electrochem. Soc. (Seattle, WA, October 1990).

8. OTHER RELATED ACTIVITIES DURING THE 1990 CONTRACT YEAR

G.D. Davis gave two lectures on surface treatments and surface analysis for Science and Technology of Adhesives, a short course for State University of New York at New Paltz (Tokyo, Japan, Jan. 1990).

G.D. Davis gave an invited presentation, "Surface Treatments of Aluminum and Titanium: From Basic Research to Production Failure Analysis," at the Intl. Conf. on Adhesion and Surface Analysis (Leicester, UK, April 1990).

G.D. Davis gave an invited lecture "Adhesive Bonding and Corrosion: Basic Principles and Applications to Aging Aircraft," for the Canadian Automated Air Traffic Control System (Ottawa, Canada, July 1990).

G.D. Davis was a co-chairman of the Symposium on Applications of Surface Analysis Methods to Environmental/Materials Interactions at the 178th Meeting Electrochem. Soc. (Seattle, WA, October 1990).

B.A. Shaw is the chairman of the 1991 NACE Research in Progress Symposium on Stainless Aluminum (Cincinnati, OH, March 1991).